Distribution Agreement

In presenting this thesis as a partial fulfillment of the requirements for a degree from Emory University, I hereby grant to Emory University and its agents the non-exclusive license to archive, make accessible, and display my thesis in whole or in part in all forms of media, now or hereafter now, including display on the World Wide Web. I understand that I may select some access restrictions as part of the online submission of this thesis. I retain all ownership rights to the copyright of the thesis. I also retain the right to use in future works (such as articles or books) all or part of this thesis.

Haorui (Davy) Song April 10, 2023

Stem-like $Tcf1^{+}PD\text{-}1^{+}CD8^{+}$ T cells are required for an optimal abscopal effect stimulated by combined radiation and anti-PD-L1 therapy

by

Haorui (Davy) Song

Zachary S. Buchwald
Adviser

Biology

Zachary S. Buchwald

Adviser

Haydn T. Kissick

Committee Member

Leila Rieder

Committee Member

2023

Stem-like $Tcf1^{+}PD\text{-}1^{+}CD8^{+}$ T cells are required for an optimal abscopal effect stimulated by combined radiation and anti-PD-L1 therapy

By

Haorui (Davy) Song

Zachary S. Buchwald

Adviser

An abstract of
a thesis submitted to the Faculty of Emory College of Arts and Sciences
of Emory University in partial fulfillment
of the requirements of the degree of
Bachelor of Science with Honors

Biology

2023

Abstract

Stem-like Tcf1$^+$PD-1$^+$CD8$^+$ T cells are required for an optimal abscopal effect stimulated by combined radiation and anti-PD-L1 therapy

By Haorui (Davy) Song

Not only a local cancer treatment, radiotherapy (RT) also induces global antitumor immunity and occasionally, the abscopal effect, an immune-mediated occurrence in which non-irradiated metastases shrink together with the irradiated tumor. Despite that the RT-induced abscopal effect could be enhanced by PD-1/PD-L1 checkpoint inhibitors, which evade T cell exhaustion by acting on tumor-infiltrating, stem-like Tcf1$^+$PD-1$^+$CD8$^+$ T cells, the immune landscape behind this combined treatment remains poorly understood. Here we show that these intratumoral Tcf1$^+$PD-1$^+$CD8$^+$ progenitor exhausted T cells are required for the optimal abscopal effect stimulated by combined RT and PD-L1 blockade. Depletion of this stem-like subset curtailed the previously enhanced abscopal effect and reversed the tumor control in both irradiated and unirradiated sites. In addition, we find that combined RT and PD-L1 inhibitors curbed tumor growth more effectively than monotherapy, and that this combined regimen expanded intratumoral Tcf1$^+$PD-1$^+$CD8$^+$ T cells, which exhibited the proliferation capacity to differentiate into more cytotoxic and terminally exhausted effector T cells. Thus, our findings reveal that the stem-like Tcf1$^+$ progenitor exhausted population may serve as a critical target for improving the clinical response to radiation and immune checkpoint blockade.

Stem-like $Tcf1^{+}PD\text{-}1^{+}CD8^{+}$ T cells are required for an optimal abscopal effect stimulated by combined radiation and anti-PD-L1 therapy

By

Haorui (Davy) Song

Zachary S. Buchwald

Adviser

A thesis submitted to the Faculty of Emory College of Arts and Sciences
of Emory University in partial fulfillment
of the requirements of the degree of
Bachelor of Science with Honors

Biology

2023

Acknowledgements

This work was supported by ASTRO-Melanoma Research Alliance awards.

No words can describe the author's immense gratitude for his caring and supportive principal investigator Dr. Zachary Buchwald, his wonderful mentors Dr. Haydn Kissick and Dr. Leila Rieder, as well as his inspiring mentors and kindhearted companions Dr. Yang Shen and Ms. Chengjing Zhou. Thank you for enkindling my passion for science and immunology, and thank you for staying by my side through all the highs and lows.

Table of Contents

INTRODUCTION

Radiotherapy (RT) and the abscopal effect

For more than a century, radiotherapy (RT) has played a critical role in cancer treatment. The use of ionizing radiation in treating cancers dates back to as early as 1896—merely one year after Röntgen discovered X-rays[1]. Since then, RT has been widely employed to curb local tumors. Although RT was traditionally viewed as a local treatment, there have been sporadic reports of the shrinkage of unirradiated metastases at distant sites concurrently with the irradiated tumor, a phenomenon first described and termed the abscopal effect (*'ab'*– away from, *'scopus'*– target) by R. H. Mole in 1953[2]. In clinical settings, the abscopal effect is uncommon: Abuodeh et al. identified a total of only 46 published case reports from 1969 to 2014[3]. Due to its rarity, the abscopal effect was considered too unpredictable to become a target for translational research[4].

Radiotherapy-induced immune responses and the immune-mediated abscopal effect

Conventionally, RT was deemed immunosuppressive, since lymphocytes are one of the most radiosensitive types of somatic cells, and whole-body radiation oftentimes leads to acquired lymphocytopenia, i.e., low total lymphocyte count[4]. Nonetheless, many experiments using mouse models revealed the immunogenicity of RT, which is mainly initiated by first, the RT-induced dsDNA breaks (DSBs), and second, the release of damage-associated molecular patterns (DAMPs) after RT-induced immunogenic cell death[4] (Figure 1).

As X-rays cause severe DNA damage in the form of double-stranded breaks, subsequent mitosis of those genomically damaged cells results in the formation of micronuclei[5]. Notably, Harding et al. found that the cyclic GMP–AMP synthase (cGAS), a pattern-recognition receptor (in particular, a DNA sensor) typically found in the cytosol, relocalized to micronuclei following

ionizing radiation, detected DNA, produced cyclic GMP-AMP (cGAMP), and activated the cGAS-STING pathway, which led to the downstream expression of type I interferons (IFNs)[5]. Multifunctional and essential to the immune system, type I IFNs increase the expression of interferon-stimulated genes (ISGs), many of which upregulate the effector function of $CD8^+$ T cells; type I IFNs also upregulate the cross-presentation of antigens (including tumor antigens) by dendritic cells (DCs), and stimulate major histocompatibility complex (MHC) class I expression on tumor cells (Figure 1). Multiple studies confirmed the RT-induced upregulation of type I IFNs and their upregulated downstream effects. For instance, Burnette et al. showed that RT significantly increased the intratumoral production of IFN-β (a member of type I IFNs) and boosted the cross-presentation capacity of intratumoral dendritic cells, while such enhancement of DCs was not seen in interferon-α/β receptor (IFNAR; the shared type I IFN receptor) knockout (KO) mice after radiation[6]. Further, Reits et al. in 2006 showed that ionizing radiation increased MHC class I expression on the surface of human melanoma cells, thereby enhancing $CD8^+$ T cells' recognition of the irradiated melanoma cells[7].

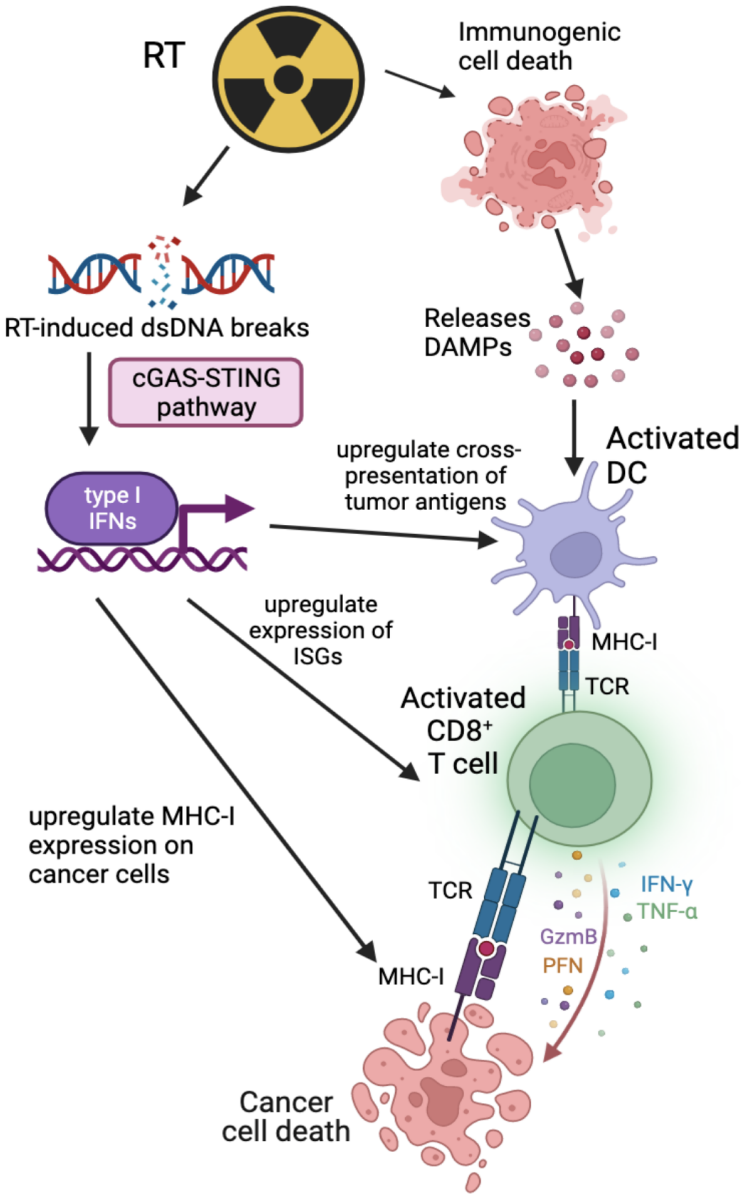

Figure 1 | Radiotherapy promotes $CD8^+$ T cell killing of cancer cells via 1) RT-induced dsDNA breaks, which activate the cGAS-STING pathway and the downstream expression of type I interferons, and 2) the release of DAMPs after immunogenic cell death that activate dendritic cells. Type I IFNs upregulate the expression of interferon-stimulated genes (ISGs) in $CD8^+$ T cells, the cross-presentation of tumor antigens by dendritic cells (DCs), and the MHC class I (MHC-I) expression on tumor cells. Once activated, $CD8^+$ T cells kill cancer cells via cytotoxic proteins such as granzyme B (GzmB) and perforin (PFN), and with the help of cytokines including interferon gamma (IFN-γ) and tumor necrosis factor alpha (TNF-α). Created in BioRender.com.

Secondly, radiation-driven immunogenic cell death entails the release of DAMPs, including a protein named high-mobility group box 1 (HMGB1), which binds to Toll-like receptor 4 (TLR4) on DCs, triggers the TLR4-dependent signaling pathway, and promotes the cross-presentation of antigens by DCs[4, 8, 9]. In other words, following radiotherapy, both DAMPs and type I IFNs act in synergy to activate dendritic cells, enabling them to better present tumor antigens to $CD8^+$ T cells, which then proceed to kill tumor cells (Figure 1). Hence, the immune responses generated by RT on multiple fronts suggest that RT can be regarded as an indirect form of immunotherapy[10].

Given that radiation can trigger immune responses, the abscopal effect—a post-radiation event—was hypothesized to relate to one's immunity. In 2004, Demaria et al. proved that the abscopal effect was indeed mediated by the immune system, and more specifically, $CD8^+$ T cells[11]. They did not observe an abscopal effect in the T cell-deficient (nude) mice after RT, whereas the abscopal effect occurred (the growth of the non-irradiated tumor was delayed) in the control mice post RT[11]. Similarly, Rodriguez-Ruiz et al. in 2016 and Buchwald et al. in 2020 confirmed that $CD8^+$ T cells were required for the abscopal effect, as *in vivo* depletion of $CD8^+$ T cells in mice using rat anti-mouse CD8 monoclonal antibody (αCD8) significantly curtailed the abscopal effect[10, 12].

T cell exhaustion and PD-1/PD-L1 checkpoint inhibitors

Chronic exposure to antigens, such as tumors and viruses, epigenetically induces T cell differentiation, resulting in terminally differentiated, exhausted $CD8^+$ T_{EX} cells with severely limited proliferation capacity[13, 14]. This phenomenon, known as T cell exhaustion, was first reported in the mouse model infected by lymphocytic choriomeningitis virus (LCMV) in 1993[15];

later, it was shown that T cell exhaustion occurred in human chronic viral infection and cancer as well[16, 17].

According to studies on the molecular signature of exhausted $CD8^+$ T_{EX} cells by researchers including Wherry et al., one of the hallmarks of T cell exhaustion is the constitutive, persistent expression of inhibitory receptors such as PD-1 (programmed cell death protein 1)[16, 18]. Notably, in exhausted T cells, even when the chronic exposure to antigens ceases, the PD-1 promoter remains demethylated and "on.[19]"

Part of the CD28 family, the transmembrane receptor PD-1 inhibits the activation of lymphocytes and contains the immunoreceptor tyrosine-based inhibitory motif (ITIM) in its cytoplasmic tail[14, 20]. After the tyrosine in an ITIM is phosphorylated, it recruits inhibitory phosphatases including SHP2 (SH2-containing phosphatase 2), which docks to the phosphorylated tyrosine residue through its SH2 (Src Homology 2) domain[14, 20]. The inhibitory phosphatase SHP2 then removes the phosphate groups of several important intermediary proteins in the T-cell receptor signal transduction pathways, including CD3-ζ, ZAP-70 (zeta-chain associated protein kinase 70), and the LAT/SLP-76 (linker for activation of T cells/SH2 domain-containing leukocyte protein of 76 kDa) complex[14, 21].

The main ligand that binds to the PD-1 receptor is a B7-family ligand named PD-L1 (programmed death ligand-1; also known as B7-H1)[14]. PD-L1 is naturally expressed on many different somatic cells. As PD-L1 binds to a PD-1 receptor, the ITIM of PD-1 becomes activated and proceeds to inhibit T cells' effector function and dampen one's immune responses (Figure 2, left panel). Such innate mechanism reflects the evolutionary advantages of immune checkpoints and the body's balancing act of fine-tuning the magnitude of immune responses. Indeed, PD-1 knockout mice (*Pdcd1*$^{-/-}$; *Pdcd1* gene encodes PD-1), which lacked the inhibitory PD-1

receptors, spontaneously developed various autoimmune diseases—an indication of overly activated immunity[22]. Unsurprisingly, however, tumor cells also take advantage of this mechanism and express PD-L1 on their cellular surfaces to repress T cell immunity: a high level of PD-L1 expression is a hallmark of cancer cells and associated with poor prognosis[23, 24, 25].

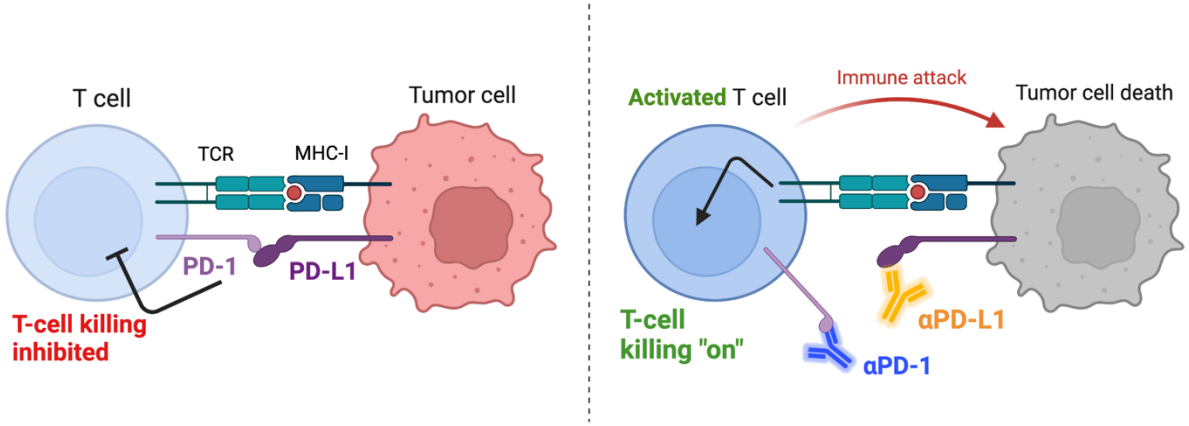

Figure 2 | PD-L1 ligands on tumor cells bind to PD-1 receptors on T cells and inhibit T cell killing; anti-PD-1 and anti-PD-L1 monoclonal antibodies block PD-L1–PD-1 binding and partially restore T cells' effector function. αPD-1 mAb, anti-PD-1 monoclonal antibodies; αPD-L1 mAb, anti-PD-L1 monoclonal antibodies. Created in BioRender.com.

Accordingly, blockade of PD-L1–PD-1 binding was hypothesized to partially remove the inhibitory signal and reactivate T cell killing of virally infected cells or tumors (Figure 2, right panel). In 2006, Barber et al. confirmed that the administration of anti-PD-1 monoclonal antibodies (αPD-1 mAb; Figure 2, right panel), which blocked the interaction of PD-L1 with PD-1, into mice chronically infected with LCMV enhanced virus-specific T cell responses[26]. In terms of tumors, Iwai et al. in 2002 showed that anti-PD-L1 monoclonal antibodies (αPD-L1 mAb; Figure 2, right panel), which too blocked the binding of PD-L1 with PD-1, rendered murine tumor cells more susceptible to the lysis of $CD8^+$ T cells and decreased mouse tumor growth *in vivo*[27].

Based on these preclinical findings, PD-1/PD-L1 checkpoint inhibitors (or checkpoint blockades) were developed pharmaceutically as a form of cancer immunotherapy. Clinical trials saw cancer patients with reduced tumor load and improved survival[28, 29]. And in 2014, the first αPD-1 mAb type of drug, Nivolumab (Opdivo®), was approved by the US Food and Drug Administration (FDA) to treat metastatic melanoma. Later, in 2016, Atezolizumab (Tecentriq®) became the first PD-L1 inhibitor approved by the FDA. To this day, clinical trials and pharmaceutical development involving PD-1/PD-L1 checkpoint inhibitors abound.

Enhancement of the abscopal effect by PD-1/PD-L1 checkpoint inhibitors

As clinical trials on PD-1/PD-L1 checkpoint inhibitors surged in numbers, researchers began to experiment with combining immunotherapy with radiotherapy in pursuit of a more robust antitumor response. In 2014, Dovedi et al. showed that αPD-1 or αPD-L1 mAbs delivered in combination with radiotherapy markedly reduced the local tumor volume and improved survival in mice—significantly more than the monotherapy treatment groups of radiotherapy alone or αPD-1/PD-L1 mAbs alone[30]. Furthermore, Park et al. reported that such synergistic effect between αPD-1/PD-L1 mAbs and RT was seen not only in the irradiated tumor site of mice, but also their unirradiated, abscopal tumors[31]. In the study, the combination of RT and PD-1 blockade led to a 66% reduction in the size of unirradiated tumors outside the radiation field, demonstrating that PD-1/PD-L1 checkpoint inhibitors in combination with RT significantly enhanced the abscopal effect, which was once considered uncommon and unpredictable[31]. Despite that clinical trials returned mixed results and have yet to confirm the findings of pre-clinical studies, over the last decade, there has been a growing consensus that combining radiotherapy with immunotherapy shows promise in boosting the abscopal effect[4, 32]. Currently,

given that the detailed mechanisms underlying the abscopal effect remain unclear, there is an urgent need for a better understanding of the effect on the immune and molecular levels in order to benefit more cancer patients.

Stem-like Tcf1$^+$PD-1$^+$CD8$^+$ T_{PEX} cells and terminally differentiated Tim-3$^+$PD-1$^+$CD8$^+$ T_{EX} cells

In 2014, Tumeh et al. described the occurrence of a proliferative burst of intratumoral CD8$^+$ T cells in patients with metastatic melanoma after they received the PD-1 checkpoint inhibitor pembrolizumab[33]. Moreover, this increment of intratumoral CD8$^+$ T cells directly correlated with a reduction in tumor volume in patients who were responsive to the PD-1 blockade[33]. Since PD-1/PD-L1 checkpoint blockades were long thought to act mainly upon terminally differentiated, exhausted CD8$^+$ T_{EX} cells with a high level of PD-1 expression, their findings, at first, seemingly contradicted the notion that CD8$^+$ T_{EX} cells had a very limited proliferation capacity. To account for this contradiction, it was then speculated that PD-1/PD-L1 blockades might function by reversing T cell exhaustion. However, chromatin-accessibility profiling (including ATAC-seq) performed by Miller et al. demonstrated that intratumoral exhausted CD8$^+$ T_{EX} cells had distinct epigenetic and transcriptional signatures, and that their exhaustion was epigenetically enforced to remain in a stable state[34]. Further, Pauken et al. showed that the epigenetic features of CD8$^+$ T_{EX} cells indeed changed little after PD-L1 blockade, suggesting that PD-1/PD-L1 blockades did not intrinsically "revitalize" CD8$^+$ T_{EX} cells, and that the observed proliferation of CD8$^+$ T cells after PD-1/PD-L1 therapy was unlikely to originate from the terminally exhausted CD8$^+$ T_{EX} cells themselves[35].

A pillar discovery, Im et al. in 2016 defined the specific subset of $CD8^+$ T cells responsible for providing the proliferative burst after PD-1 therapy[36]. They found that in chronic LCMV infection, two distinct subsets of virus-specific $CD8^+$ T cells made up the pool of PD-1-expressing $CD8^+$ T cells—first, the stem cell-like progenitor exhausted $CD8^+$ T_{PEX} cells, whose generation required the transcription factor Tcf1 (T cell factor 1; encoded by *Tcf7* gene); and second, the terminally differentiated (terminal effector) exhausted $CD8^+$ T_{EX} cells, which, unlike T_{PEX} cells, were Tcf1-negative but expressed a co-inhibitory receptor named Tim-3 (T cell immunoglobulin and mucin-domain containing-3)[36] (Figure 3). The $Tcf1^+CD8^+$ T_{PEX} cells, which expressed an intermediate amount of PD-1 ($PD\text{-}1^{int}$) and possessed high proliferation capacity, could not only undergo self-renewal, but also further differentiate into T_{EX} cells with a higher level of PD-1 expression ($PD\text{-}1^{hi}$)—a process that resembled the asymmetric division of stem cells[36] (Figure 3). Most importantly, PD-1/PD-L1 blockades significantly enhanced the proliferation of stem-like T_{PEX} cells and their differentiation into T_{EX} cells (a greater than 30-fold increase in number), yet exerted minimal effect on T_{EX} cells alone[36]. In other words, the proliferative burst of $CD8^+$ T cells post PD-1 therapy resulted from the combined effect of increased self-replenishment of T_{PEX} cells and their augmented conversion into T_{EX} cells, and therefore should be ascribed to the stem-like $Tcf1^+PD\text{-}1^+CD8^+$ T_{PEX} cells.

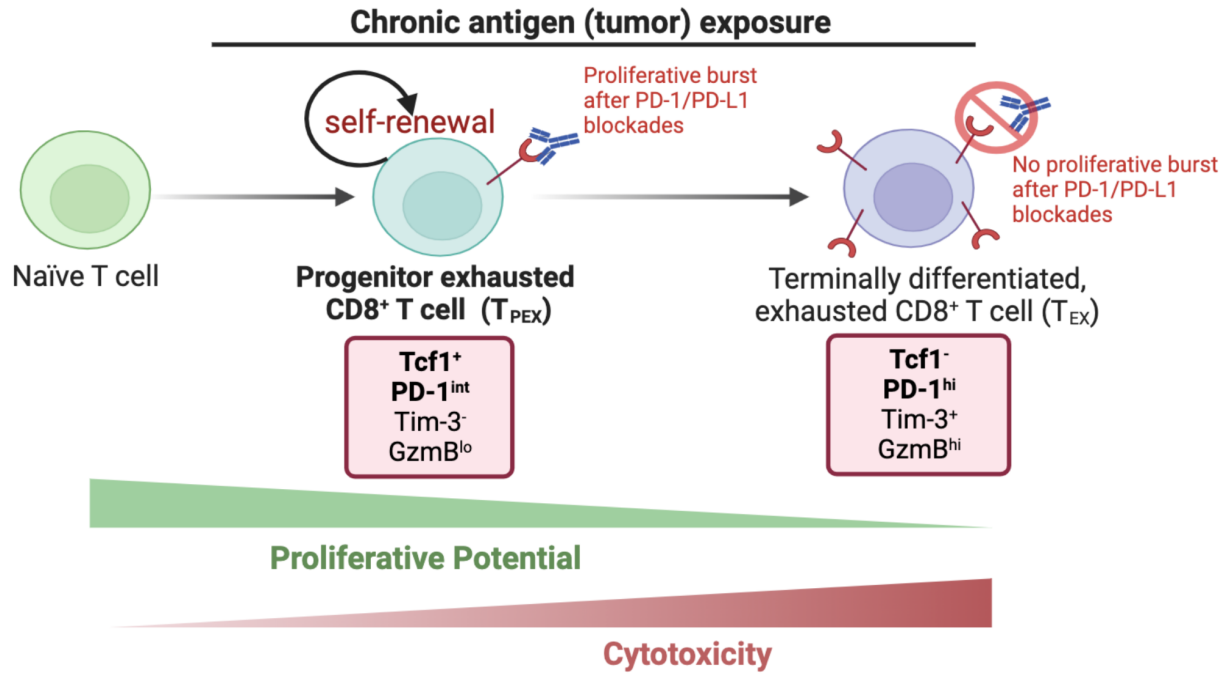

Figure 3 | In the tumor microenvironment with chronic antigen exposure, stem-like Tcf1$^+$PD-1$^+$CD8$^+$ T_{PEX} cells experience a proliferative burst after PD-1/PD-L1 checkpoint inhibitors, and are capable of both self-renewal and differentiation into terminally exhausted, short-lived Tim-3$^+$PD-1$^+$CD8$^+$ T_{EX} cells, which do not experience a proliferative burst after PD-1/PD-L1 blockades but exhibit more cytotoxicity. Although naïve CD8$^+$ T cells also express Tcf1, both T_{PEX} cells and T_{EX} cells express PD-1, a marker that helps to distinguish between the three subsets. Created in BioRender.com.

Later, Miller et al. and Siddiqui et al. confirmed Im et al.'s findings and reported similar phenomena in mouse models and melanoma patients[34, 37]. Analogous to what took place in chronic viral infections, tumor antigens too elicited two subsets of tumor-infiltrating lymphocytes—CD8$^+$ T_{PEX} and T_{EX} cells[34]. Although T_{PEX} cells express less granzyme B (GzmB^{lo}) than T_{EX} cells, are less cytotoxic, and therefore less equipped to carry out tumor-killing, they play a key role in differentiating into and maintaining the pool of T_{EX} cells, which express more granzyme B (GzmB^{hi}) and exhibit more cytotoxicity and tumor-killing capacity, yet are short-lived, more apoptotic, and less proliferative[34] (Figure 3). Moreover, Siddiqui et al.

showed that PD-1/PD-L1 checkpoint inhibitors elicited tumor control not by reversing programs of T cell exhaustion, but by acting upon $Tcf1^{+}PD\text{-}1^{+}CD8^{+}$ T_{PEX} cells, as the removal of T_{PEX} cells and the lack of Tcf1 in mice eliminated their previous responses to immunotherapy[37].

Key question

In sum, given that PD-L1 blockade enhances the abscopal effect, and that PD-L1 therapy acts on tumor-infiltrating T_{PEX} cells, we aim to investigate whether intratumoral stem-like $Tcf1^{+}PD\text{-}1^{+}CD8^{+}$ progenitor exhausted T_{PEX} cells are required for an optimal abscopal effect and tumor control in response to combined radiation and PD-L1 checkpoint inhibitor.

METHODS

Mice

All mice were used in accordance with the Emory University Institutional Animal Care and Use Committee guidelines. C57BL/6J (B6) mice and CD45.1 congenic B6 mice (B6.SJL-*Ptprc*^{a} *Pepc*^{b}/BoyJ) aged 6-8 weeks were purchased from the Jackson Laboratory. *Tcf7*$^{\text{DTR-eGFP}}$ transgenic mice were generated through CRISPR large fragment knockin (Cyagen, Inc.) and bred in house (Figure 4). P14 transgenic mice (CD45.2), which expressed T-cell receptors (TCRs; Vα2, Vβ8) specific for the lymphocytic choriomeningitis virus (LCMV) gp33 (glycoprotein residues 33-41) epitope in the context of H-2D^{b}, were crossed with *Tcf7*$^{\text{DTR-eGFP}}$ mice to generate DTR$^{+/-}$P14^{+} CD45.2 offspring. Mice were genotyped via PCR (DNA extracted from ear-punch lysates) for DTR$^{+/-}$ or DTR$^{-/-}$ and via flow cytometry (single-cell suspensions prepared from blood collection from the submandibular vein) for P14^{+} or P14^{-} (i.e., Gp33^{+} or Gp33^{-}) as well as enhanced green fluorescent protein (eGFP) expression (i.e., DTR^{+} or DTR^{-}). Female mice were used for all experiments. Mice were sacrificed if they became sick or their tumor volume reached the humane endpoint of 2 cm^{3}.

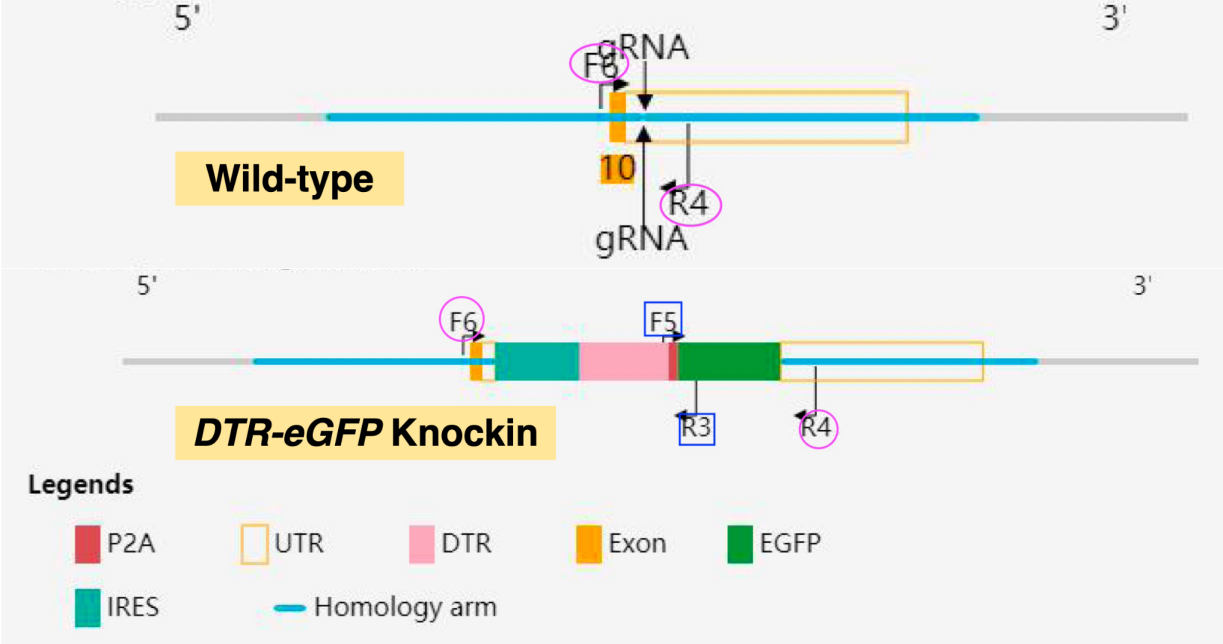

Figure 4 | CRISPR-Cas9 knockin of the *DTR-eGFP* cassette into *Tcf7* locus. The gRNA to mouse *Tcf7* gene, the donor vector containing the IRES-DTR-P2A-EGFP cassette, and Cas9 mRNA were co-injected into fertilized mouse eggs to generate knockin offspring. Following the translational stop in Exon 10 of *Tcf7* gene (located on the reverse strand of chromosome 11), the IRES-DTR-P2A-EGFP cassette was knocked in to the 3'UTR of *Tcf7*, wherein *DTR* encodes diphtheria toxin receptor (DTR), *EGFP* encodes enhanced green fluorescent protein (eGFP), *IRES* encodes internal ribosome entry site (an mRNA element that allows for translation initiation), and *P2A* encodes 2A self-cleaving peptides, which inhibits peptidyl transferase during translation.

Tumor cell lines

B16F10 melanoma cells were transfected with a minigene encoding the LCMV glycoprotein (GP) epitope. B16F10-GP cells were cultured at 37 ºC with 5% CO_2, and in Dulbecco's Modified Eagle Medium (DMEM).

Tumor implantation and tumor volume and weight measurements

Prior to tumor injection, B16F10-GP cells were counted using Trypan blue and a hemocytometer, and mixed with 10% Matrigel in RPMI 1640 medium. Both flanks of mice were shaved, the mice were anesthetized using isoflurane, and 5 x 10^5 cells were injected

subcutaneously (s.c.). Tumor volume was estimated by measuring the tumor size in two dimensions with a caliper, and calculated according to the formula $V = \frac{4}{3}\pi \times \frac{Length}{2} \times \frac{Width}{2} \times \frac{Height}{2}$. Tumors were weighed at time of sacrifice.

Adoptive T cell transfer

$P14^+$ T cells from the indicated strains of mice were obtained by grinding the spleens with the backs of syringe plungers through 70-μm cell strainers. Red blood cells were lysed with Ammonium-Chloride-Potassium (ACK) lysis buffer. Splenocytes were suspended in phosphate-buffered saline (PBS) and intravenously (i.v.) transferred to the retro-orbital sinuses of CD45.1 hosts. Since only 1/3 of the total splenocytes were $P14^+$, the total number of donor splenocytes transferred was 3 times the amount indicated in experimental designs.

Radiation

Tumor radiation was performed on the Precision X-ray Irradiator at a dose of 10 Gy using beams that were 225 kVp and run at 20 mA. During radiation, mice were anesthetized with isoflurane. To avoid scatter radiation, the radiation field was focused with a C5 collimator (5 mm). The tumor was scouted first via CT scans, based on which the treatment protocol was then designed in the SMART-ATP software.

PD-L1 blockade and diphtheria toxin (DT) treatment

For each PD-L1 blockade treatment, 200 μg of rat anti-mouse PD-L1 monoclonal antibodies (clone: 10F.9G2; isotype: rat IgG2b, κ) were injected intraperitoneally (i.p.) into each

mouse. 50 µg/kg of DT was injected intraperitoneally (i.p.) to deplete DTR-expressing cells (Figure 5).

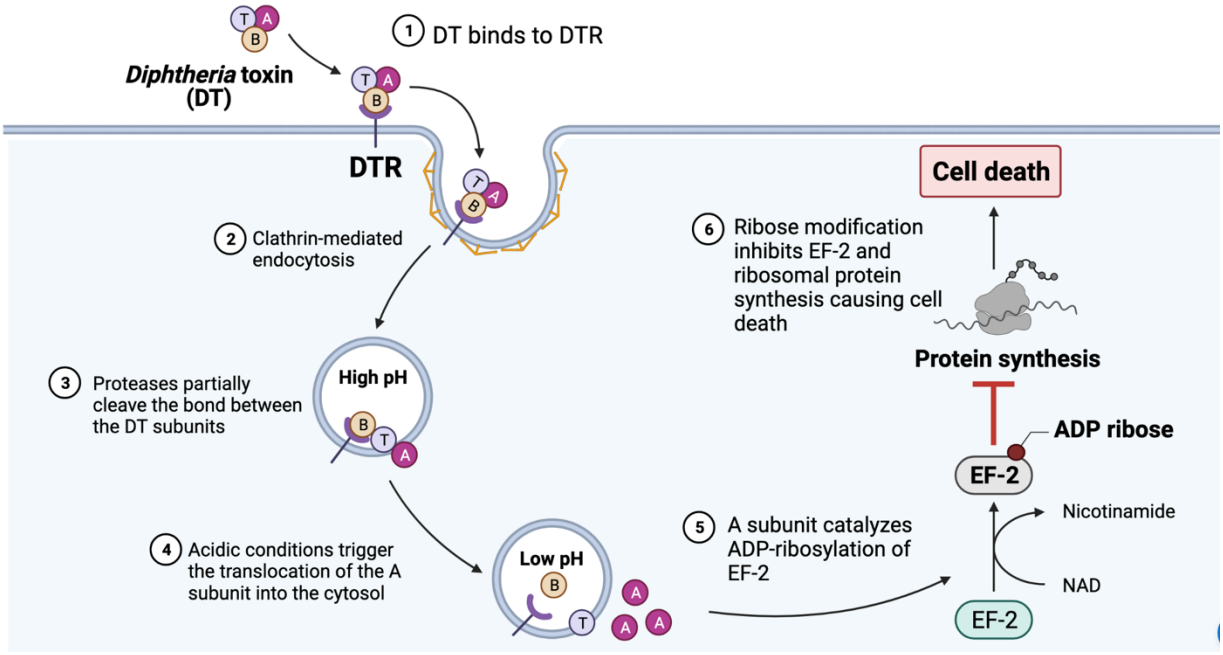

Figure 5 | Diphtheria toxin (DT) kills cells with diphtheria toxin receptor (DTR) via the ADP-ribosylation of elongation factor 2 (EF-2) and the subsequent inhibition of ribosomal protein synthesis. After the endocytosis of DT, its A subunit is cleaved by proteases, released into the cytosol, and catalyzes the ADP-ribosylation of EF-2, thus inducing apoptosis. Created in BioRender.com.

Tumor digestion and preparation of single-cell suspensions

To isolate tumor-infiltrating lymphocytes, tumors were excised, manually dissociated, and digested enzymatically in Collagenase Type IV in a shaker for 1 hour at 37 ºC. Digested tumors were mashed with the backs of syringe plungers through 70-µm cell strainers. Lymphocyte separation medium was placed at the bottom of the tubes with the help of Pasteur pipettes. After centrifugation, tumor-infiltrating lymphocytes at the interface were harvested. Single-cell suspensions of lymph nodes were obtained by grinding lymph nodes through 70-µm cell strainers with the backs of syringe plungers.

Surface and intracellular staining and flow cytometry

Surface staining was done in Flow Cytometry Staining buffer (FACS buffer) for 30 min at room temperature using fluorophore-conjugated antibodies (anti-mouse CD4–PE/Cy7, anti-mouse CD8a–PerCP-eFluor 710, anti-mouse CD45.1–BUV395, anti-mouse CD45.2–BUV563, anti-mouse Tim-3–BV711, and anti-mouse PD-1–BV605), including gp33:MHC-I (H-2D^b) tetramer–APC (Figure 6). For intracellular staining, the Foxp3/Transcription Factor Staining Buffer Set was used. Cells were then stained with intracellular fluorochrome-conjugated antibodies (anti-mouse TCF1–PE and anti-mouse GzmB–Alexa 700) in permeabilization buffer for 30 min at room temperature. Dead cells were excluded using Ghost Dye™ Red 780. Data was acquired on BD FACSymphony™ A3 flow ctyometer and analyzed in FlowJo software (version 10.8.1).

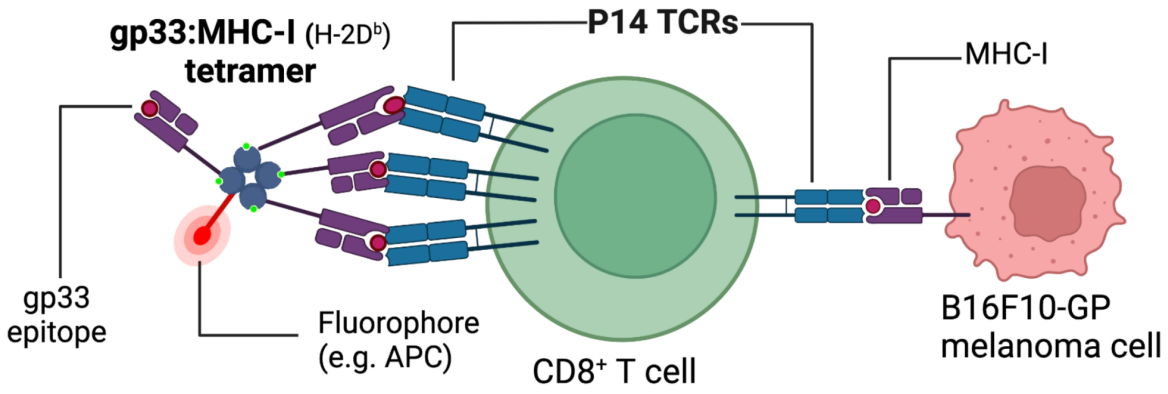

Figure 6 | Fluorophore-conjugated gp33:MHC-I tetramer complexes allows the identification of tumor-specific T cells with P14 T-cell receptors (TCRs). Since CD8$^+$ T cells only recognize peptide antigens presented in MHC class I molecules, gp33:MHC-I complexes were designed to bind to P14 TCRs and identify tumor-specific T cells via the conjugated fluorophore allophycocyanin (APC). P14 TCRs themselves bind to peptide:MHC-I complexes on the surfaces of B16F10-GP melanoma cells. H-2D^b denotes that the D region of the mouse H-2 genomic complex (on chromosome 17) encodes murine MHC class I molecules, and the C57BL/6 strain possesses the "b" allele at each MHC locus. Created in BioRender.com.

Statistical analysis

Statistical analysis was done using GraphPad Prism software (version 9.5.1). All statistical tests performed were listed in figure legends.

RESULTS

DT treatment post *DTR* gene knock-in at *Tcf7* locus depleted intratumoral and TDLN-resident Tcf1$^+$PD-1$^+$CD8$^+$ T_{PEX} cells

To investigate the roles of stem-like Tcf1$^+$PD-1$^+$CD8$^+$ T_{PEX} cells, we sought to remove only this specific subset of cells from our mouse model, so as to compare mice's responses to cancer treatments with and without the presence of this subpopulation in their immune systems. After CRISPR-Cas9 large fragment knockin of *DTR (Diphtheria toxin receptor)* gene in the form of *DTR-eGFP (enhanced green fluorescent protein)* cassette at *Tcf7* locus (which encodes Tcf1), cells expressing Tcf1 would simultaneously express DTRs on the cellular surfaces as well as eGFP (Figure 4). If diphtheria toxin (DT) was injected into the body, it would bind to DTR and deplete any DTR$^+$ cells via the inhibition of ribosomal peptide synthesis[38] (Figure 5). In our case, we expected DT treatment on DTR$^{+/-}$ mice to selectively deplete their Tcf1$^+$PD-1$^+$CD8$^+$ T_{PEX} cells, which were devised to simultaneously express DTRs. On the other hand, since mice normally do not express DTRs on any cells, DT treatment would not affect cells of DTR$^{+/-}$ mice that do not express Tcf1.

In contrast to wild-type (WT) mice without DTR expression (DTR$^{-/-}$), *DTR* knockin (KI) mice (either homozygous DTR$^{+/+}$ or heterozygous DTR$^{+/-}$) expressed the marker protein eGFP, which emitted bright green fluorescence and was detected by flow cytometry (Figure 7). Along with results from PCR (polymerase chain reaction) and gel electrophoresis, detection of the eGFP marker confirmed the successful knockin of *DTR-eGFP* cassette into *Tcf7* locus.

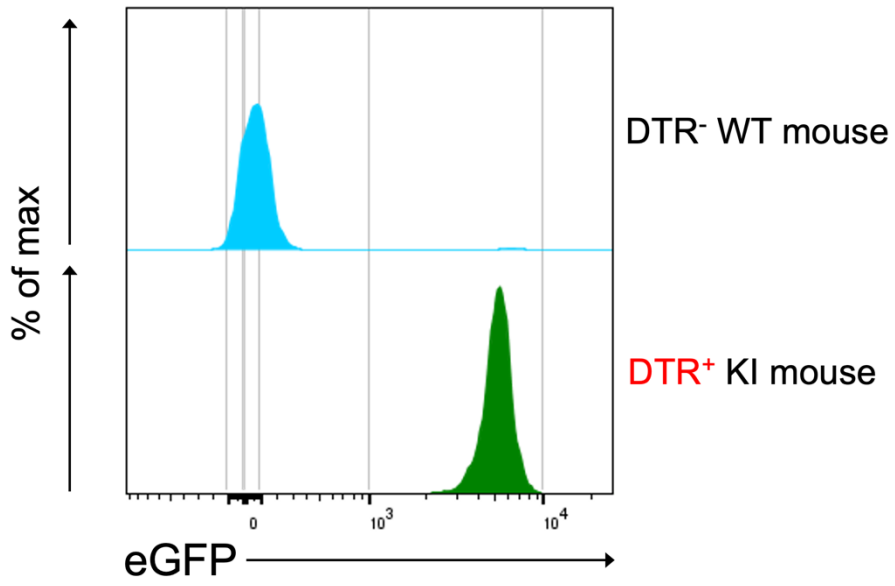

Figure 7 | ***DTR-eGFP*** **knockin mice expressed detectable eGFP.** Representative histogram flow plots of eGFP expression in a $DTR^{-/-}$ WT mouse versus a $DTR^{+/-}$ KI mouse. Cells from the DTR^{+} KI mouse exhibited eGFP fluorescence (green), whereas cells from the DTR^{-} WT mouse exhibited no eGFP fluorescence (cyan). Populations shown were gated on $CD8^{+}$ cells. Single-cell suspensions for flow cytometry were prepared from blood collection from the submandibular vein.

Next, we intended to determine whether applying DT could, in fact, deplete tumor-specific, DTR-expressing $Tcf1^{+}PD\text{-}1^{+}CD8^{+}$ T_{PEX} cells, especially those that infiltrated the tumors as well as those that resided in tumor-draining lymph nodes (TDLNs). Our tumor model involved the B16F10-GP melanoma cells, a prevalent model used in preclinical studies; and we chose melanoma due to its high immunogenicity and ability to induce adaptive immune responses[39]. The B16F10 murine melanoma cell line was generated by injecting C57BL/6J (B6) mice with B16 tumor cells, collecting *in vivo* cell growths, re-culturing, and re-injecting them into new mice for a total of 10 times. After B16F10 cells were transfected with a minigene encoding the lymphocytic choriomeningitis virus (LCMV) glycoprotein (GP) epitope, the resulting B16F10-GP cells injected *in vivo* could induce the proliferation of tumor-specific T cells, which responded to these tumor antigens. Furthermore, the tumor-specific T cells in our

P14 transgenic mice were designed to express P14 T-cell receptors (Vα2, Vβ8) that selectively bind to the gp33 segment of the glycoprotein (GP) epitope (residues 33-41: KAVYNFATC), when it is presented in the context of H-2D^{b}, a specific haplotype of murine MHC class I. Therefore, later during T-cell analysis, tumor-specific T cells (including tumor-specific T_{PEX} cells) could be identified by a flow cytometer following tetramer staining, in which fluorophore-conjugated gp33:MHC-I tetramer complexes bind to P14 T-cell receptors (TCRs) of tumor-specific T cells with high avidity and emit fluorescent signals (Figure 6). The advantage of tetramer staining lies in the fact that monomers can only weakly bind to TCRs and are easily detached from T cells, yet tetramers can achieve a stable binding.

Since we previously observed that injecting DT directly into DTR-expressing mice resulted in unexpected death (we speculated that there might be other Tcf1-expressing cells key to mice's life processes), we chose to perform adoptive transfer of splenocytes (immune cells situated in the spleen) from DTR^{+}P14^{+} CD45.2 mice to non-DTR-KI CD45.1 mice (Figures 8 and 10). CD45.2 and CD45.1 congenic mice are of the same C57BL/6 (B6) genetic background, except that one strain expresses CD45.2 tyrosine phosphatase receptors (encoded by the *Ptprc*^{b} allele), whereas the other expresses CD45.1 tyrosine phosphatase receptors (encoded by the *Ptprc*^{a} allele)[40]. This transplant model is widely employed to distinguish and track the donor and host cells, because the donor cells can circulate and proliferate in the host mice without issues of rejection; and moreover, because CD45.1 or CD45.2-expressing cells can be distinguished by flow cytometry through distinct fluorochrome-conjugated antibodies. Specifically, we intravenously injected the DTR^{+}P14^{+} CD45.2 donor cells into the CD45.1 hosts one day prior to the B16F10-GP tumor implantation, and then applied DT on the CD45.1 hosts three times to

deplete solely the DTR$^+$P14$^+$ CD45.2 donor cells without affecting the CD45.1 host cells (Figures 8 and 10).

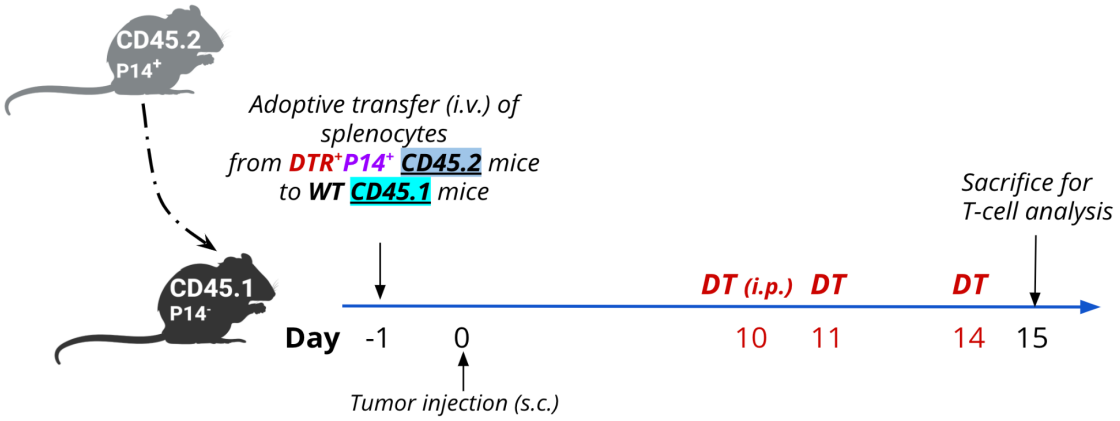

Figure 8 | Experimental design to determine whether DT would deplete tumor-specific, DTR-expressing Tcf1$^+$PD-1$^+$CD8$^+$ T_{PEX} cells in the tumor-draining lymph node (TDLN). 1 x 10^6 DTR$^+$P14$^+$ donor splenocytes from DTR$^+$P14$^+$ CD45.2 mice were intravenously (i.v.) transferred to the retro-orbital sinuses of CD45.1 hosts one day prior to subcutaneous (s.c.) B16F10-GP tumor implantation (Day 0). For the DT treatment group, 50 µg/kg of DT were intraperitoneally (i.p.) injected on Days 10, 11, and 14. Mice were sacrificed for T-cell analysis via flow cytometry on Day 15.

To examine the effect of DT on TDLN-resident T_{PEX} cells, after mice were treated according to the experimental scheme in Figure 8 and sacrificed, lymphocytes were isolated from mashed tumor-draining lymph node (TDLN) tissues. Cell events in the single-cell suspensions were recorded on the flow cytometer and afterwards gated for further analyses. Among all CD8$^+$ T cells in the CD45.1 hosts, we separated the CD45.2 donor T cells, from which we further isolated the PD-1$^+$Gp33$^+$ CD45.2 subset, which represented tumor-specific (Gp33$^+$), PD-1-expressing cells including T_{PEX} and T_{EX} cells (the gating strategy is shown in Figure 9). Analyses of Tcf1 fluorescent signals revealed that the DT treatment group (DT+) saw significant reduction (and almost complete depletion) of their Tcf1$^+$PD-1$^+$CD8$^+$ T cells in the tumor-draining lymph

node, whereas for the control group (DT-) that did not undergo DT injections, their Tcf1$^+$PD-1$^+$CD8$^+$ T cells were unaffected and preserved (Figure 9).

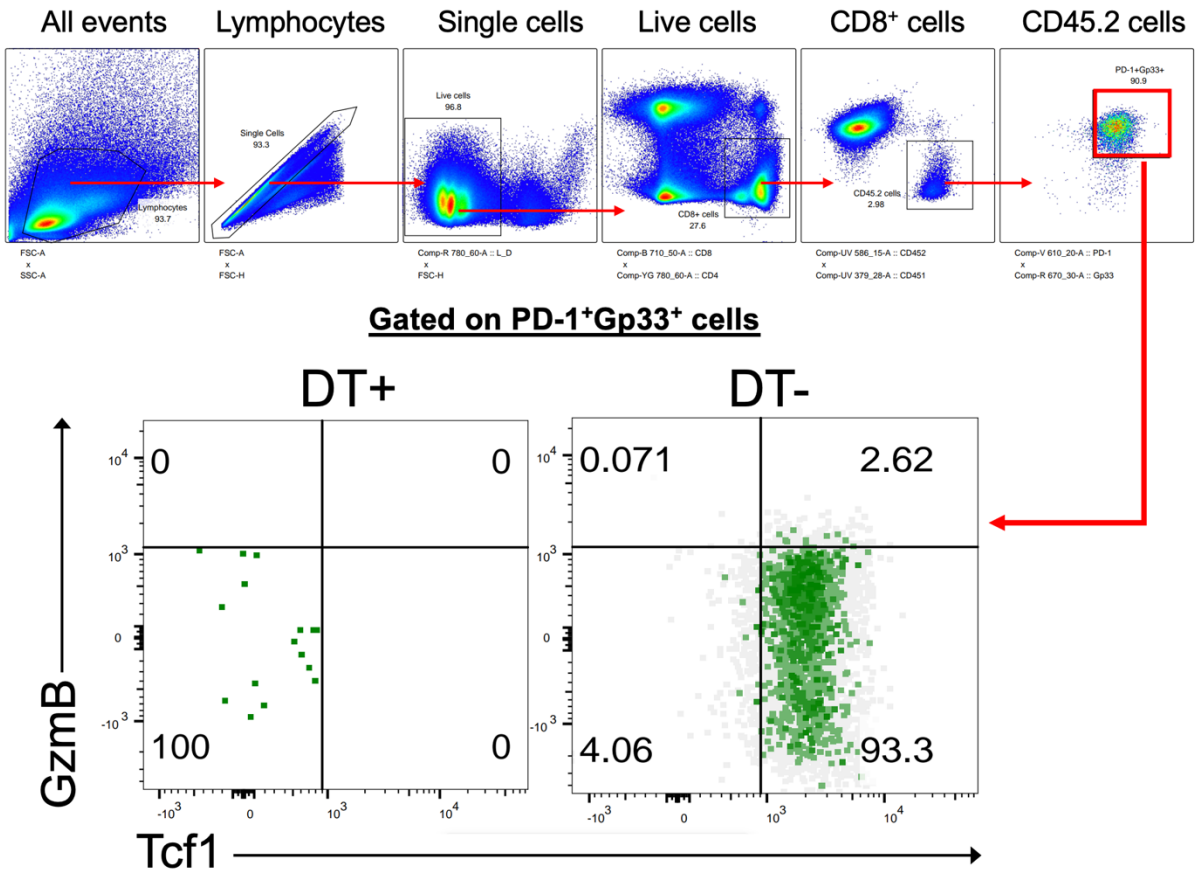

Figure 9 | DT depleted tumor-specific Tcf1$^+$PD-1$^+$CD8$^+$ T_{PEX} cells in the tumor-draining lymph node (TDLN). Representative flow plots of GzmB (granzyme B) versus Tcf1 expression for the DT treatment group (DT+; n = 3 mice) and the control group without DT treatment (DT-; n = 2 mice). Compared to the control group (DT-) with 93.3% of Tcf1$^+$ cells, DT injections (DT+) reduced the Tcf1$^+$ population to 0%. Populations shown were gated on live, CD8$^+$, CD45.2, and PD-1$^+$Gp33$^+$ cells. The gating strategy is displayed on the top.

To determine whether DT could deplete tumor-specific, DTR-expressing Tcf1$^+$PD-1$^+$CD8$^+$ T_{PEX} cells that infiltrated both primary and abscopal tumors, we subcutaneously implanted B16F10-GP tumor in bilateral flanks—and designated the right flank

as the primary tumor site and the left flank as the secondary abscopal tumor site (Figure 10). Simulating the time lag of tumor metastasis in patients, we injected the abscopal tumor 3 days after the primary tumor injection (Figure 10). After mice were sacrificed, lymphocytes were isolated from dissociated and digested tumors, recorded on the flow cytometer, and then gated using the same gating strategy delineated in Figure 9.

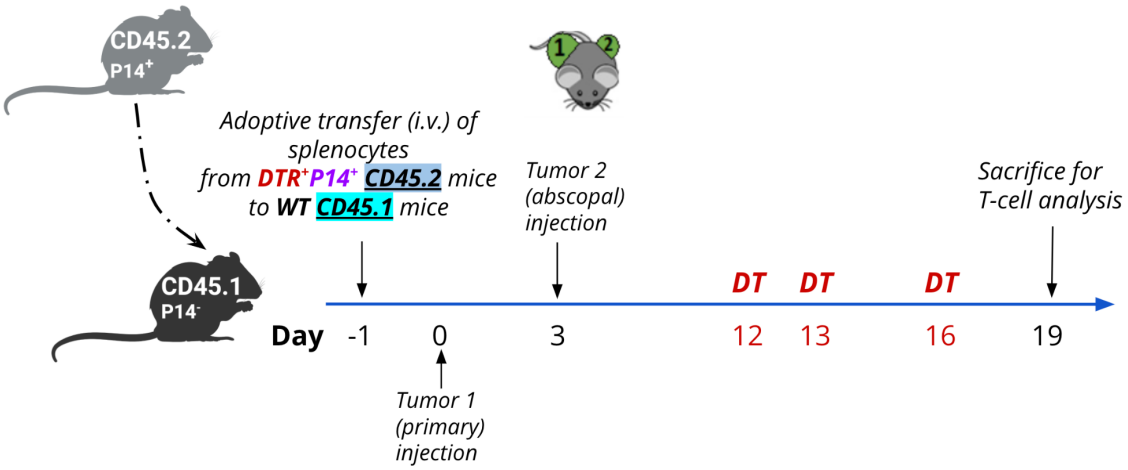

Figure 10 | Experimental design to determine whether DT would deplete tumor-infiltrating, DTR-expressing Tcf1$^+$PD-1$^+$CD8$^+$ T_{PEX} cells in both the primary and abscopal sites. 250,000 DTR$^+$P14$^+$ donor splenocytes from DTR$^+$P14$^+$ CD45.2 mice were intravenously (i.v.) transferred to the retro-orbital sinuses of CD45.1 hosts one day prior to B16F10-GP tumor implantation at the right flank, i.e., the primary site (Day 0). The secondary tumor injection on the left flank—the abscopal site—occurred on Day 3. For the DT treatment group, 50 µg/kg of DT were intraperitoneally (i.p.) injected on Days 12, 13, and 16. Mice were sacrificed for T-cell analysis via flow cytometry on Day 19.

Similar to how DT depleted TDLN-resident T_{PEX} cells, the DT treatment group (DT+) saw the tumor-specific, DTR-expressing T_{PEX} cells equally depleted in both primary and abscopal tumors, whereas no such depleting effect was observed in the control group (DT-) (Figure 11). When the PD-1$^+$Gp33$^+$ CD45.2 CD8$^+$ population was analyzed for Tim-3 versus Tcf1 expression, two subsets were separated and gated to represent the progenitor exhausted T_{PEX} subset (Tcf1$^+$Tim-3$^-$, green) and the terminally exhausted (terminal effector) T_{EX} subset

(Tim-3^{+}Tcf1^{-}, black) (Figure 11). Notably, the T_{PEX} subset that infiltrated both the primary and abscopal tumors was significantly reduced after DT injections (DT+), while the same subpopulation was unaffected without DT injections (DT-) (Figure 11). In short, diphtheria toxin treatment successfully depleted both tumor-infiltrating as well as TDLN-resident Tcf1^{+}Tim-3^{-} CD8^{+} progenitor exhausted T_{PEX} cells (which were tumor-specific and DTR-expressing).

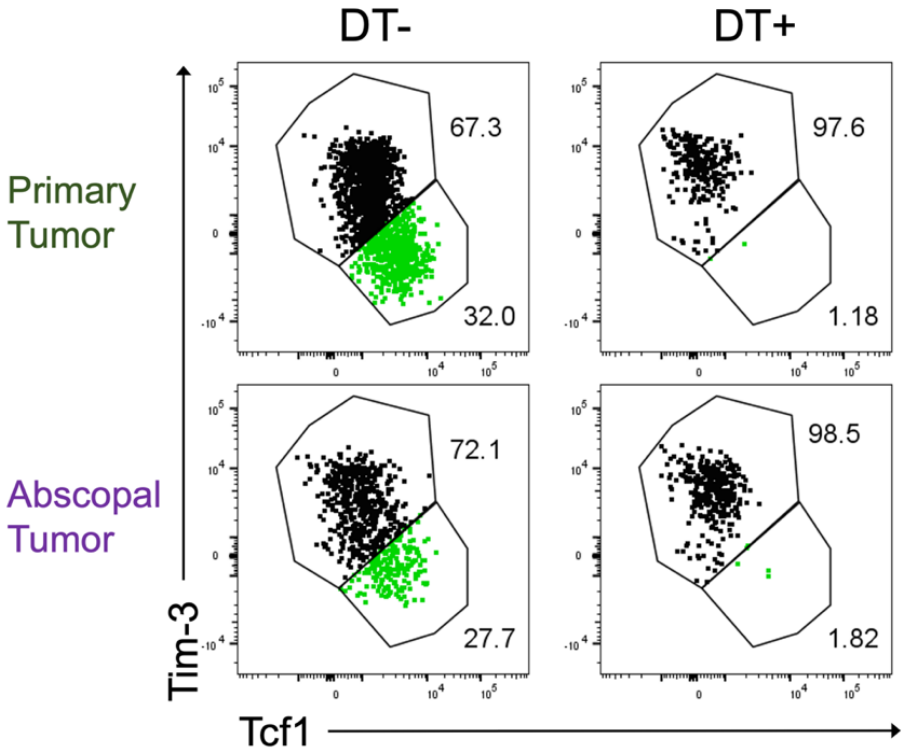

Figure 11 | DT depleted tumor-specific, intratumoral Tcf1^{+}PD-1^{+}CD8^{+} T_{PEX} cells in both the primary and abscopal sites. Representative flow plots of Tim-3 versus Tcf1 expression in both primary and abscopal tumors for the DT treatment group as well as the control group. Compared to the control group (DT-; n = 3 mice) with around 30% of Tcf1^{+}Tim-3^{-} T_{PEX} cells (green), DT injections (DT+; n = 3 mice) reduced the Tcf1^{+}Tim-3^{-} population to only approximately 1%. Populations shown were gated on live, CD8^{+}, CD45.2, and PD-1^{+}Gp33^{+} cells.

The stronger tumor control and abscopal effect stimulated by combined RT and anti-PD-L1 therapy were curtailed after depletion of Tcf1$^+$PD-1$^+$CD8$^+$ T_{PEX} cells

Since DT was able to deplete tumor-specific, DTR-expressing Tcf1$^+$PD-1$^+$CD8$^+$ T_{PEX} cells that infiltrated both primary and abscopal tumors, we then evaluated trends of tumor growths in response to various treatment groups with and without the presence of T_{PEX} cells. Expanding upon the experimental scheme depicted in Figure 10, we first performed adoptive transfer of splenocytes (among which contained T_{PEX} cells) from either DTR$^+$P14$^+$ CD45.2 or DTR$^-$P14$^+$ CD45.2 donor mice to non-DTR-KI CD45.1 hosts; accordingly, one group of CD45.1 hosts received and harbored tumor-specific DTR$^+$ T_{PEX} cells, while the other group received and harbored tumor-specific DTR$^-$ T_{PEX} cells (Figure 12). One day later, we subcutaneously implanted B16F10-GP tumor into the right flank (the primary tumor site); and the abscopal tumor was injected into the left flank three days after that to simulate the time lag of metastasis (Figure 12). We devised three treatment subgroups—RT (only), αPD-L1 (only), and RT & αPD-L1 (combined treatment); for both the RT and the RT & αPD-L1 subgroups, only the primary tumor was irradiated to observe any potential abscopal effect in the abscopal site outside the radiation field (Figure 12). To contrast tumor growth kinetics in the presence and absence of T_{PEX} cells, both DTR$^+$P14 and DTR$^-$P14 cell transfer groups were administered DT, and we expected an absence of tumor-specific T_{PEX} cells in the DTR$^+$P14 cell transfer group and a presence of tumor-specific T_{PEX} cells in the DTR$^-$P14 cell transfer group post DT treatment.

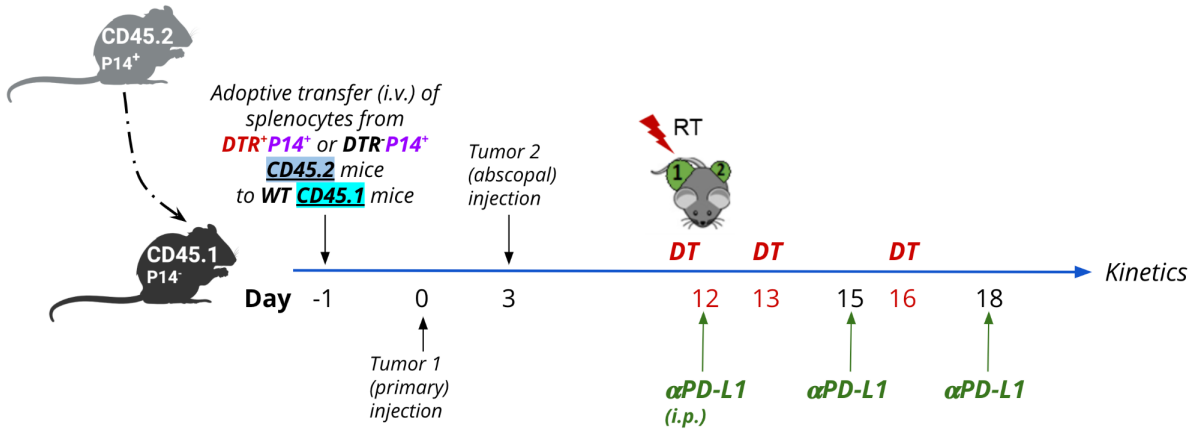

Figure 12 | Experimental design to evaluate the role of Tcf1^{+}PD-1^{+}CD8^{+} T_{PEX} cells in mediating tumor control and the abscopal effect in response to the combination of RT and αPD-L1 mAb. 250,000 DTR^{+}P14^{+} or DTR^{-}P14^{+} donor splenocytes from CD45.2 mice were intravenously (i.v.) transferred to the retro-orbital sinuses of CD45.1 hosts one day prior to subcutaneous (s.c.) B16F10-GP tumor implantation at the right flank, i.e., the primary site (Day 0). The secondary tumor injection on the left flank—the abscopal site—occurred on Day 3. All groups were administered 50 µg/kg of DT intraperitoneally (i.p.) on Days 12, 13, and 16. For the RT and the RT & αPD-L1 subgroups, only the primary tumor was irradiated once at a dose of 10 Gy on Day 12. For the αPD-L1 and the RT & αPD-L1 subgroups, 200 µg of rat αPD-L1 mAb were injected intraperitoneally (i.p.) into each mouse on Days 12, 15, and 18. Tumor growth kinetics were determined by means of tumor volume measurements.

For the DTR^{-}P14 cell transfer group, CD45.1 host mice preserved the adoptively transferred tumor-specific CD45.2 T_{PEX} cells even after DT injections. The ones that did not receive any form of antitumor treatment (the DTR- control subgroup; black, unfilled circles) experienced the fastest tumor growth at both the primary and abscopal sites—the majority of their tumor volumes rapidly exceeded the humane endpoint of 2 cm^3 and individuals must be sacrificed early on Day 20 (Figures 13A and 13B). In comparison, mice in the monotherapy subgroups, including DTR^{-} RT (turquoise, unfilled circles) and DTR^{-} αPD-L1 (blue, unfilled circles), responded to their respective treatments and experienced slower primary tumor growth rates and smaller tumor volumes on Day 20 (Figure 13A). Notably, at the abscopal site, the abscopal effect was observable in both the DTR^{-} RT and the DTR^{-} αPD-L1 subgroups on Day 20, as the mean tumor volumes were significantly lower than that of the DTR^{-} controls (Figure 13B).

More importantly, individuals that underwent the combined treatment of RT and αPD-L1 mAb (the DTR$^-$ RT & αPD-L1 subgroup; red, unfilled circles) saw their primary tumor growth significantly slowed and the tumor volumes significantly lower than those in both monotherapy subgroups on Days 20 and 23—toward the endpoint (Figure 13A). The same significant results held for the abscopal tumors, with individuals in the DTR$^-$ RT & αPD-L1 subgroup experiencing the most extensive abscopal effect and having the lowest mean tumor volume (Figure 13B).

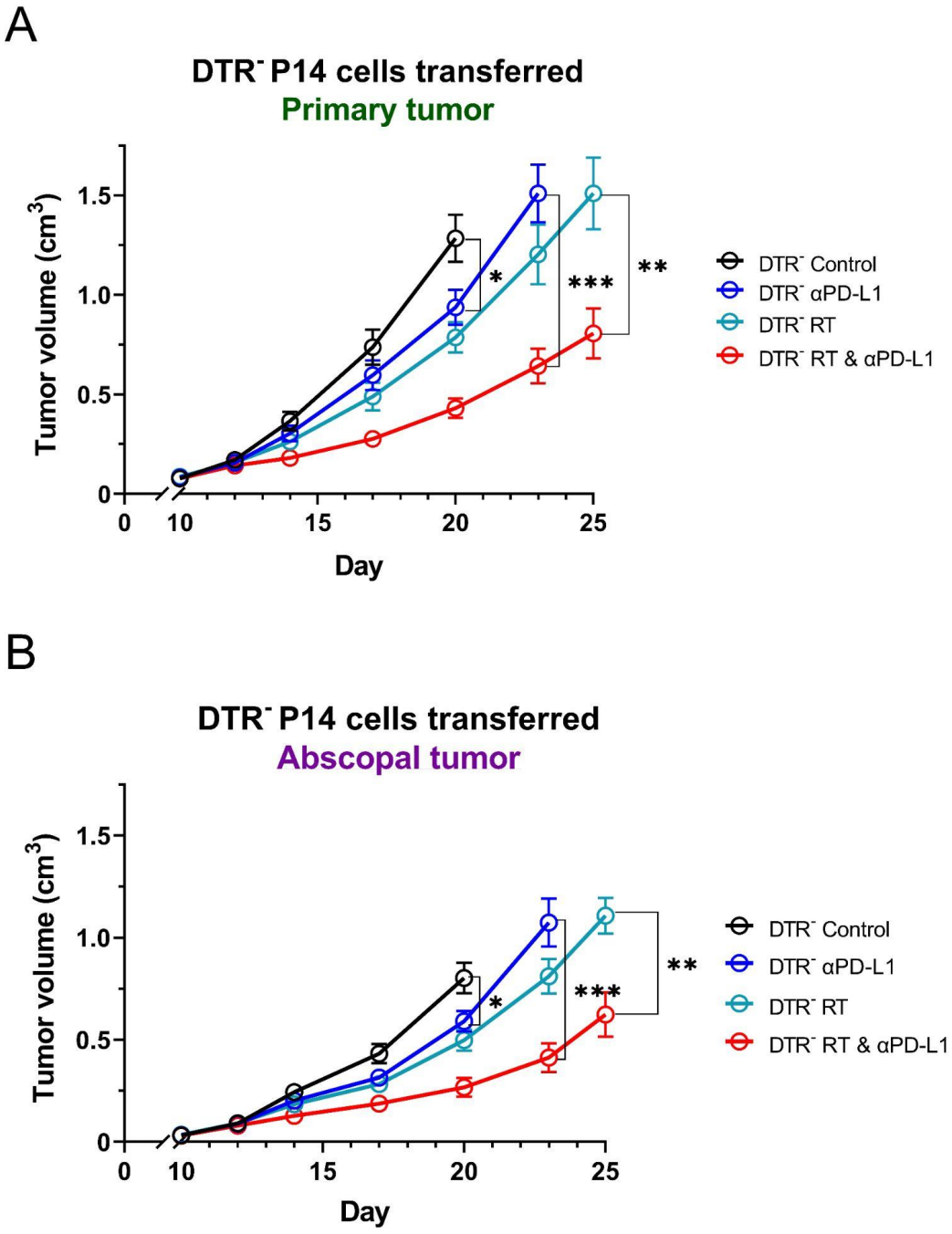

Figure 13 | In the presence of DTR⁻ T_{PEX} cells (no depletion), the combined treatment of RT and αPD-L1 mAb curbed the growth of both primary and abscopal tumors to a greater extent than monotherapy. (A) After adoptive transfer of DTR⁻P14 cells and thus no depletion of tumor-specific T_{PEX} cells, the primary tumor volume for the RT & αPD-L1 treatment subgroup (red) was significantly less than that of the RT only subgroup (turquoise) on Day 25; and likewise, significantly less in comparison to the αPD-L1 only subgroup (blue) on Day 23. (B) Similar to the trend in the primary tumor, without depletion of tumor-

specific T_{PEX} cells, the growth rate of the abscopal tumor slowed down significantly for the combined treatment subgroup (red) in comparison to either the RT only subgroup (turquoise) or the αPD-L1 only subgroup (blue).
Tumor volume was measured on Days 10, 12, 14, 17, 20, 23, and 25, if mice were alive and their tumor volume had not reached 2 cm^3 (the humane endpoint), past which they must be sacrificed. Data are combined results of 2 experiments (n = 5 mice per subgroup per experiment). Mean ± SEM (error bars represent the standard error of the mean). Multiple unpaired Student's t-tests, where ns, not significant; *P<0.05; **P<0.01; ***P<0.001.

On the contrary, for the DTR^+P14 cell transfer group, the adoptively transferred tumor-specific CD45.2 T_{PEX} cells were depleted after DT injections. As we juxtaposed and compared the DTR^- RT & αPD-L1 subgroup with the DTR^+ RT & αPD-L1 subgroup, a clear difference could be seen—on Day 25, at both primary and abscopal sites, the presence of T_{PEX} cells in the DTR^- group (red, dashed line) entailed significantly lower mean tumor volume than the lack of T_{PEX} cells in the DTR^+ group (red, solid line) (Figures 14A and 14B). This suggested that the depletion of tumor-specific $Tcf1^+PD\text{-}1^+CD8^+$ T_{PEX} cells (red, dashed line) reversed the tumor control and the abscopal effect (Figure 14B) that were significantly enhanced by the combined RT and PD-L1 therapy.

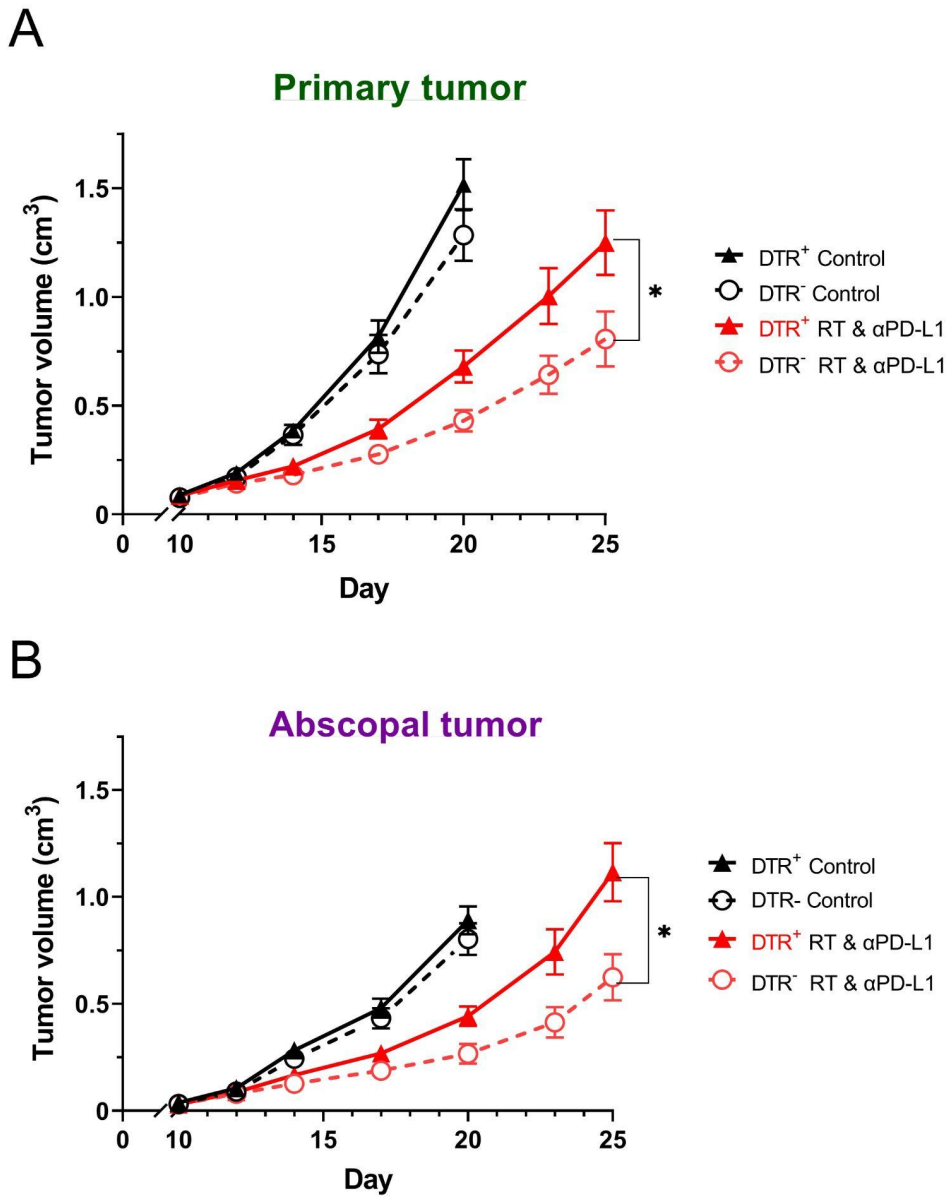

Figure 14 | After depletion of Tcf1$^+$PD-1$^+$CD8$^+$ T_{PEX} cells by DT, previous tumor control and abscopal effect in response to the combined treatment of RT and PD-L1 inhibitor were reduced.
(A) The primary tumor growth rate of the DTR$^+$ RT & αPD-L1 subgroup (tumor-specific T_{PEX} cells depleted) was significantly higher than the DTR$^-$ RT & αPD-L1 subgroup (tumor-specific T_{PEX} cells not depleted).
(B) Likewise, for abscopal tumors, the mean tumor volume of the DTR$^+$ RT & αPD-L1 subgroup (tumor-specific T_{PEX} cells depleted) was significantly higher than that of the DTR$^-$ RT & αPD-L1 subgroup (tumor-specific T_{PEX} cells not depleted).
Tumor volume was measured on Days 10, 12, 14, 17, 20, 23, and 25, if mice were alive and their tumor volume had not reached 2 cm^3 (the humane endpoint), past which they must be sacrificed. Data are combined

results of 2 experiments (n = 5 mice per subgroup per experiment). Mean ± SEM (error bars represent the standard error of the mean). Multiple unpaired Student's t-tests, where *P<0.05.

RT in combination with PD-L1 blockade augmented intratumoral GzmB^{lo}Tcf1^{+} T$_{PEX}$ cells in both primary and abscopal tumors

Lastly, to examine the effects of RT in combination with PD-L1 blockade on intratumoral Tcf1^{+}PD-1^{+}CD8^{+} T$_{PEX}$ cells, we profiled and compared the distribution of tumor-specific CD8^{+} T$_{PEX}$ and T$_{EX}$ subsets through flow cytometry. We did not perform adoptive transfer, and instead used only the wild-type C57BL/6 (B6) CD45.2 mice. Similar to the previous experimental schemes, B16F10-GP melanoma cells were implanted into the primary site first and then into the abscopal site three days after (Figure 15). Likewise, we designed three treatment groups, RT (only), αPD-L1 (only), and RT & αPD-L1 (combined treatment); and for the RT and the RT & αPD-L1 groups, only the primary tumor was irradiated, leaving the abscopal site outside the radiation field (Figure 15). After mice were sacrificed, lymphocytes were extracted from dissociated and digested tumors, run through the flow cytometer, and then gated using the same gating strategy outlined in Figure 9, except for the CD45.2 gate.

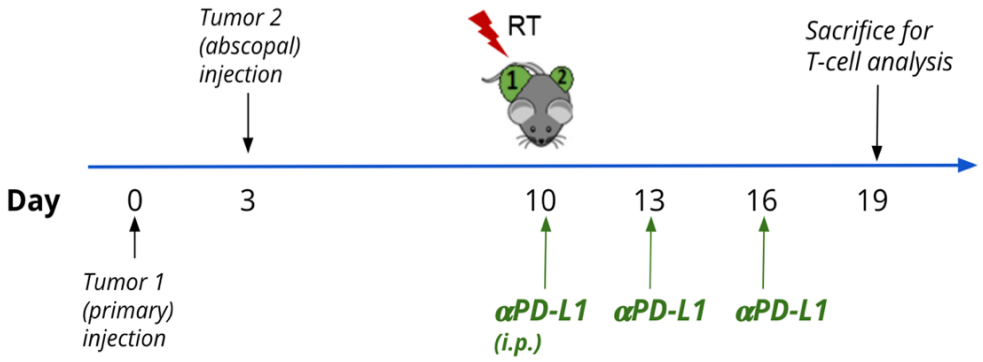

Figure 15 | Experimental design to investigate the distribution of tumor-specific CD8^{+} T$_{PEX}$ and T$_{EX}$ subsets at primary and abscopal tumor sites in response to the combination of RT and

αPD-L1 mAb. On Day 0, B16F10-GP melanoma cells were subcutaneously (s.c.) implanted at the right flank, i.e., the primary site. The secondary tumor injection on the left flank—the abscopal site—occurred on Day 3. For the RT and the RT & αPD-L1 groups, only the primary tumor was irradiated once at a dose of 10 Gy on Day 10. For the αPD-L1 and the RT & αPD-L1 groups, 200 µg of rat αPD-L1 mAb were injected intraperitoneally (i.p.) into each mouse on Days 10, 13, and 16. Mice were sacrificed for T-cell analysis via flow cytometry on Day 19.

Among the tumor-specific PD-1^{+}Gp33^{+} CD8^{+} T cells, we defined the progenitor exhausted T_{PEX} subset (Tcf1^{+}Tim-3^{-}) and the terminally exhausted (terminal effector) T_{EX} subset (Tim-3^{+}Tcf1^{-}), and calculated, for each subset, the number of cells per gram of tumor. Within the primary tumor, the number of tumor-specific, stem-like T_{PEX} cells per gram of tumor was approximately 15 times greater in mice that received the combined treatment of RT and αPD-L1 (red, filled) than those in the monotherapy groups that received only RT (turquoise, filled) or αPD-L1 (blue, filled) (Figure 16A). At the abscopal site, the number of tumor-infiltrating, stem-like T_{PEX} cells per gram of tumor for the combined treatment group (red, unfilled) was also significantly greater than the αPD-L1 only treatment group (blue, unfilled) (Figure 16A). A similar pattern was observed in the tumor-specific terminal effector T_{EX} subset. Within both the primary and the abscopal tumors, RT in combination with PD-L1 blockade gave rise to a significantly greater number of terminal T_{EX} cells per gram of tumor than only RT (Figure 16B). The concurrent increase in the number of tumor-specific T_{PEX} cells and T_{EX} cells following the combined treatment of RT and αPD-L1 suggested that the combined therapies might have triggered both the self-renewal of T_{PEX} cells and their differentiation into T_{EX} cells—hence their expansion as well—as described by Im et al.[36].

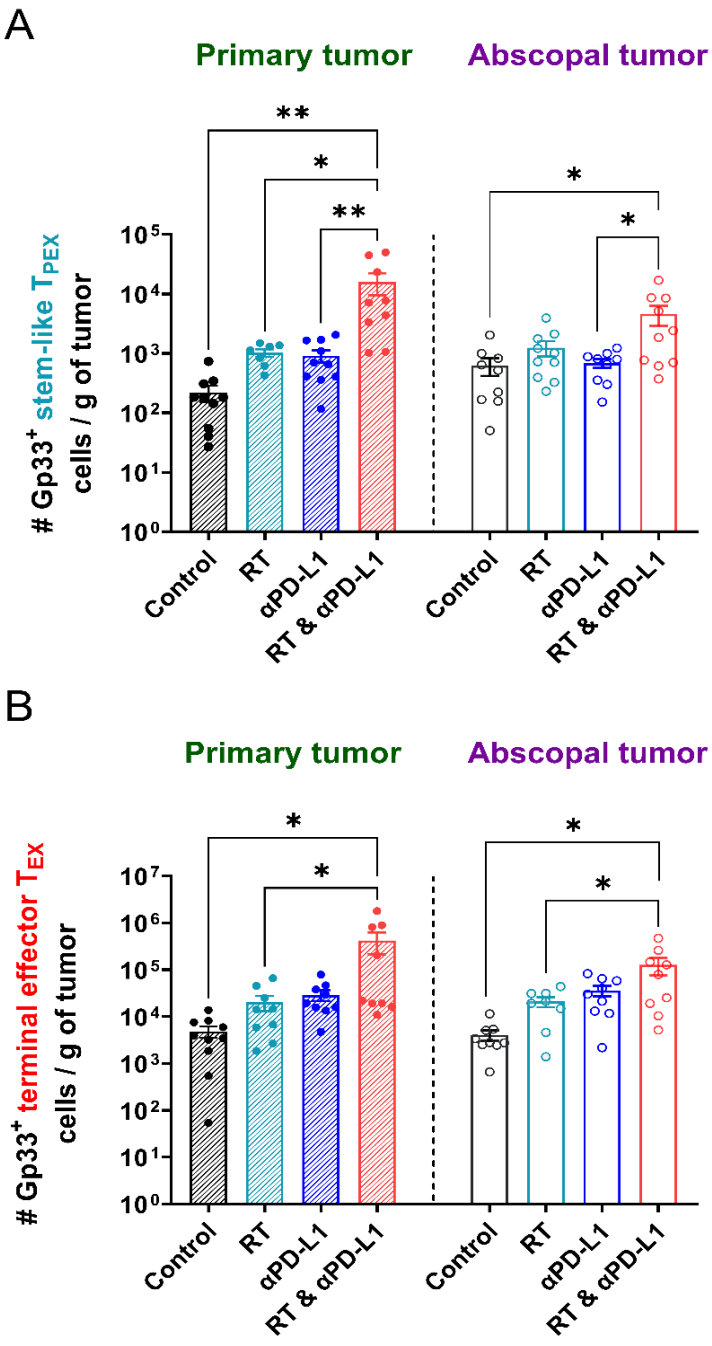

Figure 16 | Combined treatment of RT and PD-L1 therapy expanded the stem-like T_{PEX} subset as well as the terminal effector T_{EX} subset in both primary and abscopal tumors. (A) In comparison to monotherapies (RT only and αPD-L1 only), the number of tumor-specific PD-$1^{+}$$Gp33^{+}$ $Tcf1^{+}$$Tim3^{-}$ $CD8^{+}$ T cells (the stem-like T_{PEX} subset) per gram of primary tumor was significantly increased (by approximately 15-fold) after RT in combination of αPD-L1 mAb (red, filled). Additionally, the combined treatment (red, unfilled) significantly expanded the stem-like T_{PEX} population at the abscopal tumor site when compared with αPD-L1 mAb treatment only (blue, unfilled). (B) In comparison to the RT only treatment group (turquoise,

filled), the number of tumor-specific PD-1^{+}Gp33^{+} Tim3^{+}Tcf1^{-} CD8^{+} T cells (the terminal effector T_{EX} subset) per gram of primary tumor was significantly increased (by approximately 15-fold) after RT in combination of αPD-L1 mAb (red, filled). Additionally, the combined treatment (red, unfilled) significantly expanded the terminal effector T_{EX} population at the abscopal tumor site when compared with RT treatment only (turquoise, unfilled).
Data are combined results of 2 experiments (n = 5 mice per group per experiment). Mean ± SEM (error bars represent the standard error of the mean). One-way ANOVA, where *P<0.05; **P<0.01.

As we characterized the intratumoral CD8^{+} T_{PEX} and T_{EX} subsets, we noticed a visibly higher number of tumor-specific Tcf1^{+}Tim-3^{-} T_{PEX} cells in mice treated with RT in combination with αPD-L1 mAb (cyan) than mice in monotherapy groups and the control (Figure 17), which corroborated the data of the greater number of cells per gram of tumor displayed in Figure 16. Moreover, in the RT & αPD-L1 combined treatment group, tumor-specific Tcf1^{+}Tim-3^{-} T_{PEX} cells (cyan) expressed less granzyme B (GzmB^{lo}) than tumor-specific Tim-3^{+}Tcf1^{-} T_{EX} cells (red; GzmB^{hi}) at both primary and abscopal sites, indicating that the terminal effector T_{EX} subset indeed exhibited more cytotoxicity—as described by Miller et al.[34] (Figure 18).

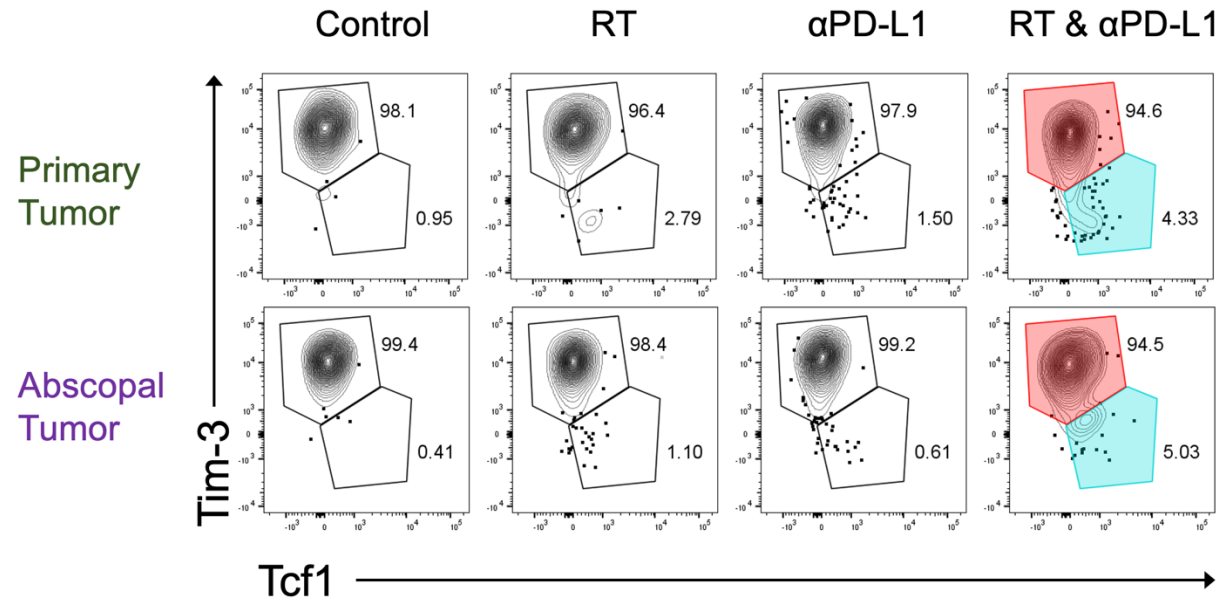

Figure 17 | Combined treatment of RT and PD-L1 blockade led to a higher number of Tcf1^{+}Tim-3^{-} T_{PEX} cells within both primary and abscopal tumors. Representative flow plots of Tim-3 versus Tcf1 expression in both primary and abscopal tumors for the three treatment groups as well as the control. Compared to the control and the monotherapy groups (RT only and αPD-L1 only), the combined

treatment group saw a higher number (approx. 4~5% versus approx. 1~2%) of Tcf1^{+}Tim-3^{-} T_{PEX} cells (cyan) within both primary and abscopal tumors. Populations shown were gated on live, CD8^{+}, and PD-1^{+}Gp33^{+} cells.

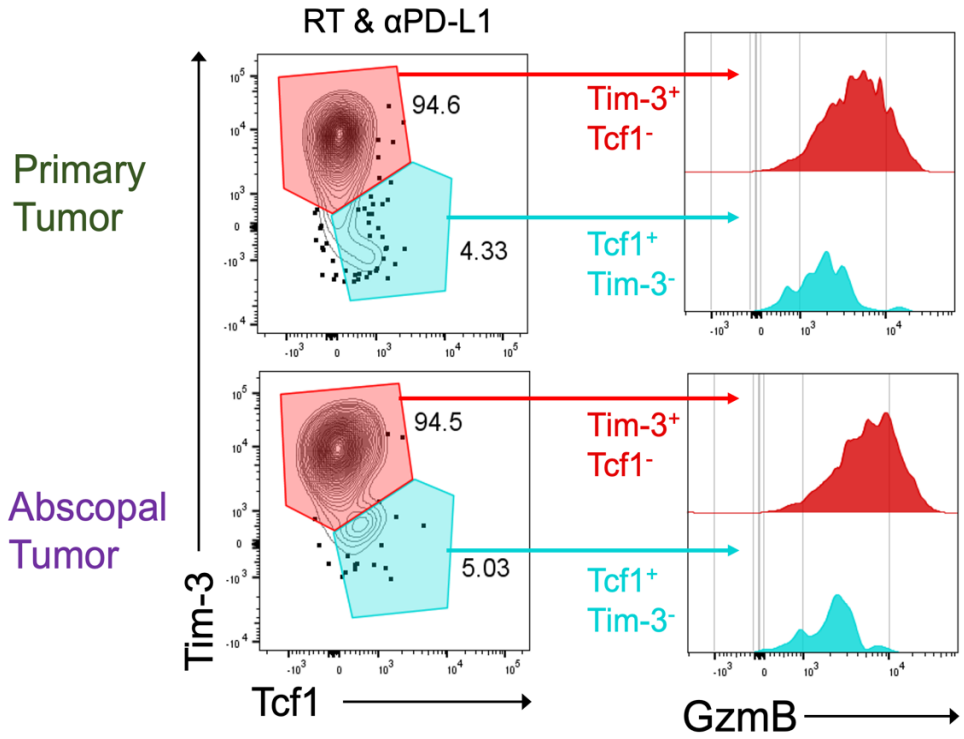

Figure 18 | Tim-3^{+}Tcf1^{-} T_{EX} cells expressed more granzyme B than Tcf1^{+}Tim-3^{-} T_{PEX} cells within both primary and abscopal tumors. Representative histogram flow plots of GzmB expression of Tim-3^{+}Tcf1^{-} (red) and Tcf1^{+}Tim-3^{-} (cyan) subsets within both primary and abscopal tumors after RT in combination with αPD-L1 mAb. At both primary and abscopal sites, tumor-specific Tim-3^{+}Tcf1^{-} T_{EX} cells expressed more GzmB (higher fluorescent signal of the right-shifted red peaks) than tumor-specific Tcf1^{+}Tim-3^{-} T_{PEX} cells. Populations shown on the left were gated on live, CD8^{+}, and PD-1^{+}Gp33^{+} cells.

DISCUSSIONS

After we confirmed that DT successfully depleted the genetically modified, DTR-expressing Tcf1$^+$PD-1$^+$CD8$^+$ T_{PEX} cells in our experimental models, we sought to connect the dots between the tumor-specific T_{PEX} subpopulation and the varying degrees of tumor control and abscopal effect in response to monotherapy (RT only or αPD-L1 mAb only) and combined therapies (RT & αPD-L1 mAb). By showing that DT depletion of T_{PEX} cells negated the enhancement of the abscopal effect by the combined treatment of RT and PD-L1 blockade, we underscored the key role of T_{PEX} cells in mediating the abscopal effect post combined therapies. Likewise, primary tumors, in the absence of intratumoral T_{PEX} cells, underwent more uncontrolled growth in the combined treatment group, indicating that the positive outcome of RT in combination with PD-L1 checkpoint inhibitor depends on the sustenance of this stem-like subset. More importantly, our data on tumor growth kinetics as well as the density of tumor-infiltrating T_{PEX} cells revealed that the combined treatment of RT and PD-L1 blockade elicited more effective tumor control and a more prominent abscopal effect than monotherapy, and that these better outcomes most likely stemmed from the proliferation of T_{PEX} cells. Stem-like T_{PEX} cells not only respond to PD-1/PD-L1 checkpoint inhibitors, but also serve as the stockpile for replenishing short-lived terminal effector T_{EX} cells, whose cytotoxicity leads to tumor cell killing. Thus, more stem-like T_{PEX} cells after the combined therapies also mean more terminal effector T_{EX} cells that can go on to induce apoptosis of cancer.

In spite of the findings described above, our study had many limitations. First, we have not yet completed the profiling and analyses of PD-1$^+$Gp33$^+$ CD45.2 CD8$^+$ T cells for the experimental scheme outlined in Figure 12. Via flow cytometry, T-cell analyses of CD45.2 host mice that received the DTR$^+$ donor cells would reveal the effect of DT on the distribution of the

T_{PEX} subset, as well as the relations between T_{PEX} cells and each treatment group (as in Figures 16 and 17). These supporting data would greatly strengthen our arguments.

Secondly, we narrowed the scope of our study to solely intratumoral $Tcf1^+PD\text{-}1^+CD8^+$ T cells, which, according to Jansen et al., reside in intratumoral antigen-presenting cell (APC) niches[41]. In fact, however, a great number of $Tcf1^+PD\text{-}1^+CD8^+$ T_{PEX} cells reside in the tumor-draining lymph nodes (TDLNs), which are critical sites for tumor-specific $CD8^+$ T cells to be primed by APCs[10]. As Buchwald et al. and Prokhnevska et al. described, TDLNs serve as the main reservoir for T_{PEX} cells, which then migrate to tumor sites in their stem-like forms and mediate adaptive immune responses[10, 42]. Since DT globally depleted our DTR-expressing T_{PEX} cells, including those in the TDLNs (Figure 9), our current data and interpretations did not address how TDLN-resident T_{PEX} cells might have impacted intratumoral T_{PEX} cells and mice's responses to anti-tumor regimens.

Finally, given that radiotherapy is known to upregulate the expression of type I interferons (IFNs), in the future, we can choose to examine the intratumoral expression of type I IFNs and how it correlates with differing tumor control in response to different treatment groups.

We believe that we had just taken one step closer to uncovering the immune mechanisms of the abscopal effect and the roles of $Tcf1^+PD\text{-}1^+CD8^+$ T_{PEX} cells in antitumor immunity. Indeed, a future where the combined regimen of radiotherapy and PD-1/PD-L1 checkpoint inhibitors realizes its full potential relies upon more researchers to join the effort with passion and commitment.

AUTHOR CONTRIBUTION

The author managed the mouse colonies and genotyped mice together with Ms. Chengjing Zhou, performed mice experiments collaboratively with Dr. Yang Shen, and collected data under the guidance of Dr. Yang Shen.

REFERENCES

1. Connell, P.P. & Hellman, S. Advances in radiotherapy and implications for the next century: a historical perspective. *Cancer Res* **69**, 383-392 (2009).
2. Mole, R.H. Whole Body Irradiation—Radiobiology or Medicine? *Br J Radiol* **26**, 234-241 (1953).
3. Abuodeh, Y., Venkat, P. & Kim, S. Systematic review of case reports on the abscopal effect. *Curr. Probl. Cancer* **40**, 25-37 (2016).
4. Janopaul-Naylor, J.R., Shen, Y., Qian, D.C. & Buchwald, Z.S. The Abscopal Effect: A Review of Pre-Clinical and Clinical Advances. *Int J Mol Sci* **22** (2021).
5. Harding, S.M. *et al.* Mitotic progression following DNA damage enables pattern recognition within micronuclei. *Nature* **548**, 466-+ (2017).
6. Burnette, B.C. *et al.* The Efficacy of Radiotherapy Relies upon Induction of Type I Interferon-Dependent Innate and Adaptive Immunity. *Cancer Research* **71**, 2488-2496 (2011).
7. Reits, E.A. *et al.* Radiation modulates the peptide repertoire, enhances MHC class I expression, and induces successful antitumor immunotherapy. *J Exp Med* **203**, 1259-1271 (2006).
8. Apetoh, L. *et al.* Toll-like receptor 4-dependent contribution of the immune system to anticancer chemotherapy and radiotherapy. *Nat Med* **13**, 1050-1059 (2007).
9. Galluzzi, L., Buque, A., Kepp, O., Zitvogel, L. & Kroemer, G. Immunogenic cell death in cancer and infectious disease. *Nat Rev Immunol* **17**, 97-111 (2017).
10. Buchwald, Z.S. *et al.* Tumor-draining lymph node is important for a robust abscopal effect stimulated by radiotherapy. *J Immunother Cancer* **8** (2020).

11. Demaria, S. *et al.* Ionizing radiation inhibition of distant untreated tumors (abscopal effect) is immune mediated. *Int J Radiat Oncol* **58**, 862-870 (2004).

12. Rodriguez-Ruiz, M.E. *et al.* Abscopal Effects of Radiotherapy Are Enhanced by Combined Immunostimulatory mAbs and Are Dependent on CD8 T Cells and Crosspriming. *Cancer Research* **76**, 5994-6005 (2016).

13. Sen, D.R. *et al.* The epigenetic landscape of T cell exhaustion. *Science* **354**, 1165-1169 (2016).

14. Hashimoto, M. *et al.* CD8 T Cell Exhaustion in Chronic Infection and Cancer: Opportunities for Interventions. *Annu Rev Med* **69**, 301-318 (2018).

15. Moskophidis, D., Lechner, F., Pircher, H. & Zinkernagel, R.M. Virus persistence in acutely infected immunocompetent mice by exhaustion of antiviral cytotoxic effector T cells. *Nature* **362**, 758-761 (1993).

16. Day, C.L. *et al.* PD-1 expression on HIV-specific T cells is associated with T-cell exhaustion and disease progression. *Nature* **443**, 350-354 (2006).

17. Baitsch, L. *et al.* Exhaustion of tumor-specific CD8(+) T cells in metastases from melanoma patients. *J Clin Invest* **121**, 2350-2360 (2011).

18. Wherry, E.J. *et al.* Molecular signature of CD8+ T cell exhaustion during chronic viral infection. *Immunity* **27**, 670-684 (2007).

19. Youngblood, B. *et al.* Chronic virus infection enforces demethylation of the locus that encodes PD-1 in antigen-specific CD8(+) T cells. *Immunity* **35**, 400-412 (2011).

20. Schildberg, F.A., Klein, S.R., Freeman, G.J. & Sharpe, A.H. Coinhibitory Pathways in the B7-CD28 Ligand-Receptor Family. *Immunity* **44**, 955-972 (2016).

21. Yokosuka, T. *et al.* Programmed cell death 1 forms negative costimulatory microclusters that directly inhibit T cell receptor signaling by recruiting phosphatase SHP2. *J Exp Med* **209**, 1201-1217 (2012).

22. Wang, J. *et al.* Establishment of NOD-Pdcd1(-/-) mice as an efficient animal model of type I diabetes. *P Natl Acad Sci USA* **102**, 11823-11828 (2005).

23. Carlsson, J. *et al.* PD-L1 Expression is Associated With Poor Prognosis in Renal Cell Carcinoma. *Appl Immunohistochem Mol Morphol* **28**, 213-220 (2020).

24. Gu, X. *et al.* Elevated PD-L1 expression predicts poor survival outcomes in patients with cervical cancer. *Cancer Cell Int* **19**, 146 (2019).

25. Noronha, C. *et al.* PD-L1 tumor expression is associated with poor prognosis and systemic immunosuppression in glioblastoma. *J Neurooncol* **156**, 453-464 (2022).

26. Barber, D.L. *et al.* Restoring function in exhausted CD8 T cells during chronic viral infection. *Nature* **439**, 682-687 (2006).

27. Iwai, Y. *et al.* Involvement of PD-L1 on tumor cells in the escape from host immune system and tumor immunotherapy by PD-L1 blockade. *Proc Natl Acad Sci U S A* **99**, 12293-12297 (2002).

28. Brahmer, J.R. *et al.* Safety and activity of anti-PD-L1 antibody in patients with advanced cancer. *N Engl J Med* **366**, 2455-2465 (2012).

29. Topalian, S.L. *et al.* Safety, activity, and immune correlates of anti-PD-1 antibody in cancer. *N Engl J Med* **366**, 2443-2454 (2012).

30. Dovedi, S.J. *et al.* Acquired Resistance to Fractionated Radiotherapy Can Be Overcome by Concurrent PD-L1 Blockade. *Cancer Research* **74**, 5458-5468 (2014).

31. Park, S.S. *et al.* PD-1 Restrains Radiotherapy-Induced Abscopal Effect. *Cancer Immunol Res* **3**, 610-619 (2015).

32. Ngwa, W. *et al.* Using immunotherapy to boost the abscopal effect. *Nat Rev Cancer* **18**, 313-322 (2018).

33. Tumeh, P.C. *et al.* PD-1 blockade induces responses by inhibiting adaptive immune resistance. *Nature* **515**, 568-571 (2014).

34. Miller, B.C. *et al.* Subsets of exhausted CD8+ T cells differentially mediate tumor control and respond to checkpoint blockade. *Nat Immunol* **20**, 326-336 (2019).

35. Pauken, K.E. *et al.* Epigenetic stability of exhausted T cells limits durability of reinvigoration by PD-1 blockade. *Science* **354**, 1160-1165 (2016).

36. Im, S.J. *et al.* Defining CD8+ T cells that provide the proliferative burst after PD-1 therapy. *Nature* **537**, 417-+ (2016).

37. Siddiqui, I. *et al.* Intratumoral Tcf1+PD-1+CD8+ T Cells with Stem-like Properties Promote Tumor Control in Response to Vaccination and Checkpoint Blockade Immunotherapy. *Immunity* **50**, 195-211.e110 (2019).

38. Murphy, J.R. Mechanism of Diphtheria Toxin Catalytic Domain Delivery to the Eukaryotic Cell Cytosol and the Cellular Factors that Directly Participate in the Process. *Toxins* **3**, 294-308 (2011).

39. Passarelli, A., Mannavola, F., Stucci, L.S., Tucci, M. & Silvestris, F. Immune system and melanoma biology: a balance between immunosurveillance and immune escape. *Oncotarget* **8**, 106132-106142 (2017).

40. Chisolm, D.A. *et al.* Defining Genetic Variation in Widely Used Congenic and Backcrossed Mouse Models Reveals Varied Regulation of Genes Important for Immune Responses. *Immunity* **51**, 155-+ (2019).

41. Jansen, C.S. *et al.* An intra-tumoral niche maintains and differentiates stem-like CD8 T cells. *Nature* **576**, 465-+ (2019).

42. Prokhnevska, N. *et al.* CD8(+) T cell activation in cancer comprises an initial activation phase in lymph nodes followed by effector differentiation within the tumor. *Immunity* **56**, 107-124 e105 (2023).